Draft version February 6, 2022
Typeset using LaTeX **modern** style in AASTeX62

arXiv:2008.13724v1 [astro-ph.HE] 31 Aug 2020

Supernova Interaction with a Dense Detached Shell in SN 2001em

Poonam Chandra,[1,*] Roger A. Chevalier,[2] Nikolai Chugai,[3]
Dan Milisavljevic,[4] and Claes Fransson[5]

[1] *National Centre for Radio Astrophysics, Tata Institute of Fundamental Research Ganeshkhind, Pune 411007, India*
[2] *Department of Astronomy, University of Virginia, P.O. Box 400325 Charlottesville, VA 22904-4325, USA*
[3] *Institute of Astronomy of Russian Academy of Sciences Pyatnitskaya St. 48, 109017 Moscow, Russia*
[4] *Department of Physics and Astronomy, Purdue University 525 Northwestern Avenue, West Lafayette, IN 47907*
[5] *Oskar Klein Centre, Department of Astronomy, Stockholm University AlbaNova, SE-106 91 Stockholm, Sweden*

(Received May xx, 2020; Revised January xx, 2020; Accepted February 6, 2022)

Submitted to ApJ

ABSTRACT

We carry out a comprehensive analysis of supernova SN 2001em covering a period of 19 years since discovery. SN 2001em is the oldest supernova known to have undergone a metamorphosis from a stripped envelope to an interacting supernova. An early spectrum indicates it exploded as a Type Ib supernova. Later, the ejecta caught up with a dense circumstellar H-shell, ejected a few thousand years before the explosion, triggering interaction between the supernova ejecta and the dense shell, producing radio, X-ray and Hα emission. We use archival data with the Very Large Array in radio bands and with *Chandra*, *XMM*-Newton and *Swift*-XRT in X-ray bands, along with published Hα measurements. We combine these data with our low radio frequency observations with the Giant Metrewave Radio Telescope at two epochs covering three frequencies. While the observations missed the phase when the shock entered the dense shell, the X-rays indicate that the shock came out of the dense shell at around 1750 days. The data suggest a forward shock origin of the X-ray emission. Radio data show a spectral inversion at late epochs (> 5000 d) at around 3 GHz, which mimics the properties of the central absorbed component seen in SN 1986J. A possible explanation for this component is that the progenitor of SN 2001em was a massive binary system which had undergone a period of common envelope evolution.

Corresponding author: Poonam Chandra
poonam@ncra.tifr.res.in

The hydrogen envelope from the SN 2001em progenitor may have been lost as a result of binary interaction.

Keywords: supernovae: general — supernovae: individual (SN 2001em) — circumstellar matter — techniques: interferometric. — radiation mechanisms: general — radiation mechanisms: non-thermal

1. INTRODUCTION

Traditional classification of supernovae divides them into categories, Type II or Type I, based on presence or absence of hydrogen, respectively, in their optical spectra (Filippenko 1997). A particular subclass of Type I supernovae, Type Ib/c supernovae (SNe Ib/c), are believed to arise from massive stars that have lost their hydrogen envelopes. While the mechanisms for outer envelope ejections are poorly understood, winds (Puls et al. 2008), episodic ejections (Smith & Owocki 2006; Pastorello et al. 2007a; Shiode & Quataert 2014), binary interactions (Smith 2014), and common envelope formation and ejection (Chugai & Chevalier 2006; Chevalier 2012) are some of the favoured scenarios. An extreme example of this subclass of supernovae are Type Ic supernovae, which not only have shed their hydrogen envelope, but the helium envelope is also lost from the progenitor. They are also known as stripped envelope supernovae and have also gained attention because of their connection with gamma ray bursts (GRBs, Modjaz et al. 2016).

In the class of hydrogen rich Type II supernovae, the subclass Type IIn supernovae are identified by their dense circumstellar interaction, and hence are also called interacting supernovae. SNe IIn can come from a variety of progenitors as long as they are surrounded by a dense circumstellar medium (CSM).

With the advent of more sensitive and automated survey telescopes, a large number of supernovae are being discovered and followed up, challenging the traditional picture of supernovae classification. The boundaries between various supernova subclasses are merging. Of particular interest in this work are stripped envelope supernovae (SNe Ib/c) that metamorphose into interacting supernovae (SNe IIn). The most straightforward reason for this metamorphosis is that the supernova ejecta are interacting with the dense hydrogen and/or helium shell(s) that were ejected during late stellar evolution. The presence of an early stripped envelope supernova phase implies that the exploding star had a fast wind phase just before the supernova.

The CSM in the vicinity of a supernova is shaped mainly by the winds from the progenitor star before explosion. Since supernova ejecta velocities are $10 - 100$ times faster than the CSM wind velocities, one can unravel the pre-explosion progenitor mass-loss history spanning thousands of years and possibly see the signatures of the ejected hydrogen and/or helium envelope shells during the late stellar evolution stages.

* Swarna Jayanti Fellow, Department of Science & Technology, India

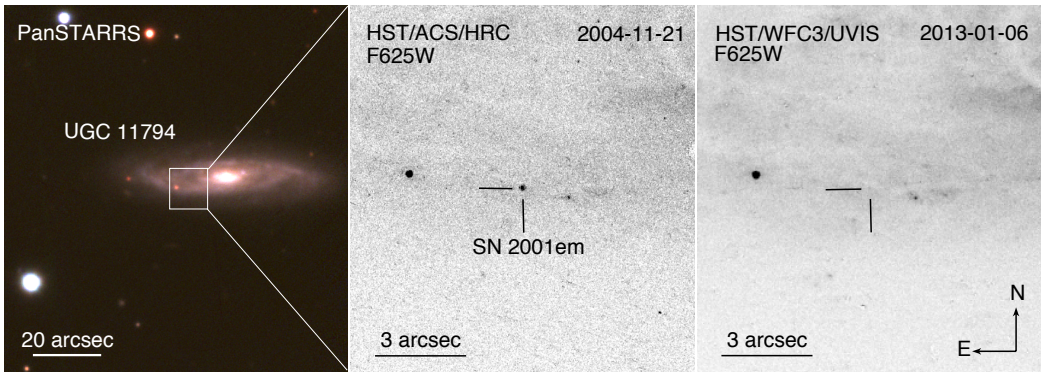


Figure 1. Archival optical images of SN 2001em and its host galaxy UGC 11797. Left: composite image of the region using PanSTARRS g, r, and i images. Middle: *Hubble Space Telescope* (*HST*) image (Proposal ID 10272; PI: A. Filippenko) obtained with the Advanced Camera for Surveys in the High Resolution Camera mode in the F625W filter sensitive to Hα, which is the dominant emission line at this epoch. Right: *HST* image (Proposal ID 13029; PI: A. Filippenko) obtained with the Wide Field Camera 3 using the same F625W filter, when SN 2001em is no longer visible.

The age at which the ejecta catch up to the shells indicates the time before the explosion when the shell was ejected. The ejecta - CSM interaction manifests itself mainly in non-thermal radio, thermal/non-thermal X-ray and Hα emission, and thus provides a unique way to constrain the progenitor evolution by unraveling its mass-loss history.

SN 2001em exploded in an outer spiral arm of the galaxy UGC 11797 ($d = 81.2 \pm 5.7$ Mpc; Grogin & Geller 2000, Figure 1). It was discovered by Papenkova et al. (2001) using the Katzman Automatic Imaging Telescope on 2001 September 20.3 and 21.3 UT. The estimated explosion date is between September 10.3 UT and September 15.3 UT (Papenkova et al. 2001); in this paper we adopt 2001 September 13 UT as the explosion date. SN 2001em was classified as a Type Ib/c supernova from optical spectra obtained on 2001 October 20 (Filippenko & Chornock 2001), approximately one month after explosion.

SN 2001em was initially a normal supernova and was not followed early on with a good cadence. However, due to its classification as a stripped-envelope supernova, some of which are known to be associated with GRBs, Stockdale et al. (2004) and Pooley & Lewin (2004) carried out late time radio and X-ray observations to determine whether the supernova harboured a misaligned GRB. If so, it could be detected at late times because the GRB jet would have slowed down with time and have become quasi-spherical, coming into our line of sight. Such a quasi-spherical jet interacting with the surrounding medium is likely to produce detectable radio and X-ray emission. SN 2001em was indeed detected in both radio and X-ray bands, initially attracting interest in the possibility that a misaligned GRB had been detected from it (Granot & Ramirez-Ruiz 2004). However, the observed high 8 GHz radio luminosity ($L_{\rm radio} \sim 2 \times 10^{28}$ erg s^{-1} Hz^{-1}) and the unabsorbed 0.3–10 keV X-ray

luminosity ($L_{\rm Xray} \sim 10^{41}$ erg s^{-1}) were unprecedented for SNe Ib/c at this age, but were comparable to the luminosities of bright SNe IIn at a similar age (Chandra 2018). Later, multiple Very Long Baseline Array (VLBA) measurements covering epochs between 2004 July to 2004 November (Stockdale et al. 2005; Paragi et al. 2005; Bietenholz & Bartel 2005; Schinzel et al. 2008) showed no extended radio emission, although its size was predicted to be ≥ 2 mas in an off-axis GRB model (Granot & Ramirez-Ruiz 2004). These observations also indicated the derived velocities to be inconsistent with a relativistically expanding radio source in SN 2001em, but were consistent with an isotropic expansion velocity of $\leq 20,000$ km s^{-1}.

The issue was resolved by Chugai & Chevalier (2006), who modeled the SN emission in the framework of the interaction of the supernova ejecta with a dense, 3 $M_\odot$ circumstellar (CS) shell at a distance of $\sim 7 \times 10^{16}$ cm formed by vigorous mass loss from the progenitor star with a rate of $(2-10) \times 10^{-3}$ M$_\odot$ yr^{-1} at $(1-2) \times 10^3$ yr prior to explosion. In their model the hydrogen envelope was completely lost and subsequently swept up and accelerated by the fast wind of the pre-supernova star up to a velocity of $30-50$ km s^{-1}. This model was also supported by the optical spectroscopy of the supernova on 2004 May 07 carried out by Soderberg et al. (2004) revealing the dominance of a broad Hα emission line with a FWHM velocity of ~ 1800 km s^{-1}, also later seen by van Dyk (2010) in their 2004 Dec 12 observations with LRIS on the Keck telescope. The detection of Hα emission was not predicted in the off-axis GRB model and was suggestive of a strong interaction with the CSM. This was further confirmed by Bietenholz & Bartel (2007), who carried out VLBI observations on 2006 May 27, 5 years after the explosion. They found that the SN was still unresolved, with a nominal size constraint of $R = (9 \pm 15) \times 10^{16}$ cm, consistent with a non-relativistic expansion of the radio emitting shock with an average expansion speed of 5800 ± 10000 km s^{-1}. The above arguments conclusively established that the origin of radio, X-ray and Hα emission in SN 2001em was due to the interaction of the ejecta with the dense hydrogen shell.

The results of Chugai & Chevalier (2006) were based on early first 1000 days of data and it remained to be seen whether the supernova was still interacting with the dense hydrogen shell or had come out of it. In this paper, we carry out a comprehensive analysis of all available X-ray and radio data, including late time Giant Metrewave Radio Telescope (GMRT) observations of SN 2001em. Although SN 2001em lacks early observations, it is the oldest SN showing a metamorphosis from a stripped-envelope supernova to an interacting supernova. As more supernovae are being discovered showing such a metamorphosis, SN 2001em presents an opportunity to study the properties of progenitors of such supernovae for a long time into the pre-explosion. In §2, we use the available optical data to classify SN 2001em. The organization of this paper is as follows: the observations are described in §3. We carry out modeling of the data and discuss our main results in §4. The discussion and analysis of our results

in the context of other similar SNe are in §5. Finally, we give our main conclusions in §6.

2. EARLY CLASSIFICATION OF SN 2001EM

There is an ambiguity in the initial classification of SN 2001em as either a Type Ib or a Type Ic supernova. In addition, observations of the intermediate stages between H-deficient to H-dominated emission in SN 2001em are limited. We inspected the only known optical spectrum of SN 2001em obtained prior to strong interaction, observed by Filippenko & Chornock (2001) and published in Shivvers et al. (2019). We confirmed the general Type Ib/c classification but found overall consistency in features more in line with a Type Ib supernova (Figure 2). Faithful comparison is complicated by not knowing the exact phase of SN 2001em when the spectrum was obtained, the poor signal-to-noise of the spectrum, and a lack of additional epochs by which to follow the evolution of features.

Given that the SN 2001em spectrum was obtained within a month of the estimated explosion date, it is reasonable to assume that the phase was within three weeks of maximum light. We compared the spectrum of SN 2001em to that of SN 2014C at the phase +8 days after maximum published in Mauerhan et al. (2018a). Most P Cyg features are shared between the objects, except at wavelengths below 5400 Å where the signal-to-noise is poor and no strong features are observed in SN 2001em. This further confirms the Type Ib nature of SN 2001em and suggests a close association between the two supernovae.

However, a noticeable difference between the spectra is that weak excess emission is seen around locations of He I lines in SN 2001em that is not observed in SN 2014C. A narrow emission feature centered around 7055 Å, potentially associated with slightly blueshifted He I 7065 and having a velocity width of ~ 1000 km s^{-1}, is particularly conspicuous. Strong narrow helium emission lines are a characteristic of Type Ibn supernovae, which are suspected of being explosions that strongly interact with He-rich environments (Pastorello et al. 2007b; Smith 2017). A spectrum of SN 2006jc is shown (Foley et al. 2007) for comparison, with conspicuous He I lines identified. The normally dominant He I λ5876 emission line is noticeably absent from SN 2001em. However, for a narrow range of phases, He I λ7065 can be the strongest He I line in Type Ibn supernovae (Karamehmetoglu et al. 2019). Although the strong P Cyg features and lack of blue continuum in SN 2001em disqualify it as a Type Ibn supernova, the consistency in He I emission locations suggests that SN 2001em may have been weakly interacting with He-rich CSM shortly after explosion. If true, this scenario would be consistent with the notion that the progenitor star of SN 2001em had strong He-rich winds that helped shape the cavity interior to the H-rich shell in the millennia approaching core collapse.

3. OBSERVATIONS

3.1. *GMRT radio observations*

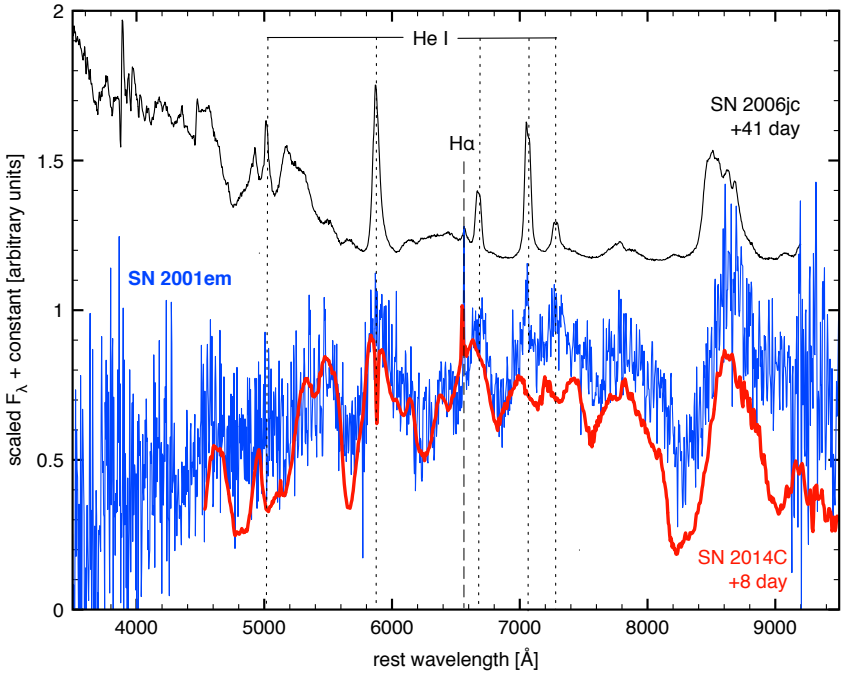


Figure 2. The optical spectrum of SN 2001em shows features consistent with Type Ib supernovae. Excess emission is potentially seen around the locations of He I lines, especially around the He I λ7065 line where it is narrow ($\sim$ 1000 km s^{-1}). This suggests that SN 2001em may have been interacting with a He-rich CSM environment prior to strong interaction with the H-rich shell. The weak signal-to-noise of the spectrum and lack of additional epochs to follow evolution of the features prevents positive identification.

We observed SN 2001em with the GMRT on 2004 February 13 at 1.3 GHz. The data were recorded in two polarizations with 16 MHz bandwidth, split into 128 channels. The observations were carried out in total intensity mode, and the data were acquired with an integration time of 16.1 sec. The data were analysed using the AIPS software. Initial flagging and calibration were done using the software FLAGCAL, developed for automatic flagging and calibration for the GMRT data (Prasad & Chengalur 2012). The flagged and calibrated data were closely inspected; further flagging and calibration were done manually until the data quality looked satisfactory. The calibration solutions of a single channel were applied to the full bandwidth. Several channels were averaged together to take care of the effect of bandwidth smearing. Fully calibrated data of the target source were imaged using the AIPS task IMAGR. A few rounds of self-calibration were performed.

We also observed SN 2001em with the upgraded GMRT in frequency band 3 (250–500 MHz), band 4 (550–900 MHz) and band 5 (1000–1450 MHz) in December 2019. The data were recorded with 10 s integration time and the bandwidth was divided into 2048 channels. The data were analysed using standard Common Astronomy Software Applications (CASA) packages (McMullin et al. 2007), following the methodology of Kale et al. (2018).

The flux density of the SN was found by fitting a Gaussian at the SN position using the AIPS task JMFIT. The details of the GMRT observations and the flux density values can be found in Table 3.2. For carrying out the fitting and analysis, we add 10% uncertainty in quadrature, a typical calibration uncertainty in the GMRT data (Chandra & Kanekar 2017).

3.2. *Very Large Array radio observations*

The Very Large Array (VLA) observations started in October 2003 and continued until July 2020. The data from the years 2003 to 2008 were obtained with the old VLA covering the frequency range $1.4 - 22.5$ GHz. The data were taken in standard continuum mode with a total bandwidth 2×50 MHz. We used the Astrophysical Image Processing System (AIPS) to analyse the VLA data. We analysed all publicly available archival VLA data in order to obtain consistent flux density values. Our reanalysed values match with the published flux densities whenever available.

The later data were taken with the upgraded Karl G. Jansky Very Large Array (JVLA). We carried out JVLA data analysis using the standard packages within the Common Astronomy Software Applications package (CASA). The details of observations and the flux density values can be found in Table 3.2. We add 10% error in the quadrature to the flux density values for analysis purposes, a typical uncertainty in the flux density calibration scale at the observed frequencies [1].

[1] https://science.nrao.edu/facilities/vla/docs/manuals/oss/performance/fdscale

Table 1. Radio observations of SN 2001em

Date of Observation (UT)	Telescope Configuration[b]	Proposal ID	Age[a] (day)	Frequency (GHz)	Resolution $''\times''$	Flux density mJy	Ref.
2003 Oct 17	VLA:B	AS779	764	8.46	$0.89'' \times 0.62''$	0.899 ± 0.036	This paper
2004 Jan 31	VLA:BC	AW617	870	1.43	$16.72'' \times 4.80''$	< 0.654	This paper
”	”	”	”	4.86	$4.49'' \times 1.40''$	1.596 ± 0.081	This paper
”	”	”	”	8.46	$2.25'' \times 2.12''$	1.340 ± 0.043	This paper
”	”	”	”	14.94	$1.63'' \times 0.43''$	0.859 ± 0.219	This paper
2004 Feb 13	GMRT	05PCA02	883	1.29	$3.92'' \times 2.39''$	< 0.478	This paper
2004 Mar 23	VLA:C	AW617	922	1.43	$17.77'' \times 12.99''$	< 1.154	This paper
”	”	”	”	4.86	$4.13'' \times 3.80''$	1.552 ± 0.043	This paper
”	”	”	”	8.46	$2.58'' \times 2.12''$	1.595 ± 0.042	This paper
”	”	”	”	14.94	$1.49'' \times 1.23''$	0.958 ± 0.140	This paper
2004 Apr 20	VLA:C	AW624	950	1.43	$14.45'' \times 13.72''$	< 0.645	This paper
”	”	”	”	4.86	$4.18'' \times 3.90''$	1.784 ± 0.054	This paper
”	”	”	”	8.46	$2.39'' \times 2.30''$	1.655 ± 0.054	This paper
2004 Jul 01	VLBA	...	1022	8.46	$0.0019'' \times 0.0008''$	1.8 ± 0.2	Stockdale+04
2004 Sep 10	VLA:A	AW642	1093	1.43	$1.30'' \times 1.26''$	0.416 ± 0.064	This paper
”	”	”	”	4.86	$0.38'' \times 0.37''$	1.773 ± 0.062	This paper
”	”	”	”	8.46	$0.21'' \times 0.21''$	1.678 ± 0.047	This paper
”	”	”	”	14.94	$0.13'' \times 0.12''$	0.826 ± 0.205	This paper
”	”	”	”	22.46	$0.09'' \times 0.08''$	0.897 ± 0.118	This paper
2004 Nov 22	VLBA	...	1166	8.46	$0.0009'' \times 0.0009''$	1.5 ± 0.1	Bietenholz+04

Table 1 continued on next page

Table 1 *(continued)*

Date of Observation (UT)	Telescope Configuration[b]	Proposal ID	Age[a] (day)	Frequency (GHz)	Resolution $''\times''$	Flux density mJy	Ref.
2005 Feb 07	VLA:AB	AW641	1243	1.43	$4.42'' \times 1.42''$	0.862 ± 0.169	This paper
"	"	"	"	4.86	$1.31'' \times 0.45''$	1.752 ± 0.267	This paper
"	"	"	"	8.46	$0.76'' \times 0.25''$	1.430 ± 0.060	This paper
2005 Feb 25	VLA:B	GB053	1261	1.43	$4.74'' \times 4.49''$	0.845 ± 0.267	This paper
"	"	"	"	8.46	$0.78'' \times 0.73''$	1.456 ± 0.085	This paper
"	"	"	"	14.94	$0.45'' \times 0.40''$	< 0.990	This paper
"	"	"	"	22.46	$0.31'' \times 0.26''$	1.282 ± 0.288	This paper
2005 Mar 11	e-VLBI	...	1275	1.6	$0.0024'' \times 0.0024''$	~ 0.88	Paragi+05
2005 Mar 24	VLA:B	AW641	1288	1.43	$4.30'' \times 4.09''$	1.037 ± 0.235	This paper
"	"	"	"	4.86	$1.26'' \times 1.20''$	2.161 ± 0.074	This paper
"	"	"	"	8.46	$0.77'' \times 0.64''$	1.601 ± 0.051	This paper
2005 Apr 26	VLA:B	AW641	1321	1.43	$4.38'' \times 3.96''$	1.039 ± 0.146	This paper
"	"	"	"	4.86	$1.26'' \times 1.18''$	2.001 ± 0.070	This paper
"	"	"	"	8.46	$0.72' \times 0.68''$	1.477 ± 0.037	This paper
2005 May 23	VLA:B	AW641	1348	1.43	$4.26'' \times 3.85''$	1.307 ± 0.304	This paper
"	"	"	"	4.86	$1.20'' \times 1.13''$	1.694 ± 0.138	This paper
"	"	"	"	8.46	$0.67'' \times 0.65''$	1.349 ± 0.082	This paper
2005 Jun 13	VLA:BC	AW642	1369	14.94	$1.47'' \times 0.44''$	1.274 ± 0.164	This paper
"	"	"	"	22.46	$0.95'' \times 0.29''$	0.995 ± 0.101	This paper
2005 Jun 14	VLA:BC	AW647	1370	1.43	$14.80'' \times 4.87''$	1.352 ± 0.119	This paper
"	"	"	"	4.86	$4.20'' \times 1.43''$	1.968 ± 0.049	This paper
"	"	"	"	8.46	$2.64'' \times 0.78''$	1.523 ± 0.033	This paper

Table 1 continued on next page

Table 1 *(continued)*

Date of Observation (UT)	Telescope Configuration[b]	Proposal ID	Age[a] (day)	Frequency (GHz)	Resolution $''\times''$	Flux density mJy	Ref.
”	”	”	”	22.46	$1.00'' \times 0.30''$	0.788 ± 0.110	This paper
2005 Jul 12	VLA:C	AW641	1398	1.43	$14.52'' \times 13.85''$	1.522 ± 0.284	This paper
”	”	”	”	4.86	$4.08'' \times 3.86''$	1.931 ± 0.059	This paper
”	”	”	”	8.46	$2.39'' \times 2.26''$	1.432 ± 0.054	This paper
2005 Aug 12	VLA:C	AW641	1429	4.86	$4.00'' \times 3.70''$	1.883 ± 0.039	This paper
”	”	”	”	8.46	$2.34'' \times 2.21''$	1.443 ± 0.033	This paper
2006 Apr 17	VLA:A	AW675	1677	1.43	$1.36'' \times 1.12''$	1.214 ± 0.105	This paper
”	”	”	”	4.86	$0.49'' \times 0.33''$	1.586 ± 0.073	This paper
”	”	”	”	8.46	$0.23'' \times 0.19''$	1.016 ± 0.058	This paper
”	”	”	”	22.46	$0.09'' \times 0.07''$	0.649 ± 0.127	This paper
2006 May 27	VLBI	...	1717	8.4	0.0017” $\times$ 0.0008”	1.05 ± 0.06	BB+07
2006 May 27	VLA:AB	BB219	1717	1.43	$12.70'' \times 2.16''$	1.282 ± 0.205	This paper
”	”	”	”	22.46	$0.76'' \times 0.12''$	< 0.765	This paper
2006 Aug 30	VLA:B	AW679	1812	1.43	$4.39'' \times 4.04''$	1.606 ± 0.081	This paper
”	”	”	”	4.86	$1.30'' \times 1.20''$	1.063 ± 0.047	This paper
”	”	”	”	8.46	$0.71'' \times 0.69''$	0.749 ± 0.038	This paper
2007 Feb 04	VLA:CD	BG162	1970	8.46	$6.82'' \times 3.15''$	0.715 ± 0.173	This paper
2007 Feb 18	VLA:CD	STUDEN	1984	1.43	$42.31'' \times 37.88''$	< 1.337	This paper
”	”	”	”	4.86	$11.74'' \times 10.31''$	1.019 ± 0.165	This paper
”	”	”	”	22.46	$2.54'' \times 2.18''$	0.453 ± 0.083	This paper
2007 May 29	VLA:A	AW709	2084	1.43	$1.47'' \times 1.28''$	1.075 ± 0.050	This paper
”	”	”	”	4.86	$0.42'' \times 0.34''$	0.913 ± 0.095	This paper

Table 1 continued on next page

Table 1 *(continued)*

Date of Observation (UT)	Telescope Configuration[b]	Proposal ID	Age[a] (day)	Frequency (GHz)	Resolution $''\times''$	Flux density mJy	Ref.
”	”	”	”	14.94	$0.13'' \times 0.12''$	< 0.780	This paper
2008 Sep 25	VLA:A	AS961	2569	4.86	$0.41'' \times 0.37''$	0.604 ± 0.048	This paper
2008 Oct 01	VLA:A	AS961	2575	1.43	$1.24'' \times 1.22''$	0.939 ± 0.095	This paper
”	”	”	”	8.46	$0.22'' \times 0.21''$	0.298 ± 0.030	This paper
”	”	”	”	22.46	$0.10'' \times 0.08''$	0.336 ± 0.099	This paper
2016 Aug 26	VLA:B	SH746	5461	3.04	$2.01'' \times 1.71''$	0.062 ± 0.016	This paper
”	”	”	”	8.55	$0.74'' \times 0.63''$	0.095 ± 0.012	This paper
”	”	”	”	9.04	$0.71'' \times 0.59''$	0.095 ± 0.009	This paper
”	”	”	”	11.06	$0.60'' \times 0.49''$	0.104 ± 0.011	This paper
2019 Dec 22	uGMRT	37_097	6674	0.40	8.22” × 5.44”	< 0.204	This paper
”	”	”	”	0.65	4.24” × 3.62”	0.149 ± 0.051	This paper
2019 Dec 23	”	”	6675	1.26	2.57” × 1.66”	0.107 ± 0.045	This paper
2020 Jun 29	JVLA	20A_124	6865	6.0	2.02” × 0.97”	0.050 ± 0.010	This paper
2020 Jun 29	JVLA	20A_124	6865	10.0	0.64” × 0.59”	0.065 ± 0.010	This paper
2020 Jun 30	JVLA	20A_124	6866	32.99	0.19” × 0.17”	0.056 ± 0.011	This paper
2020 Jul 05	JVLA	20A_124	6871	15.30	0.44” × 0.36”	0.075 ± 0.008	This paper
2020 Jul 15	JVLA	20A_124	6881	2.81	2.13” × 2.02”	< 0.075	This paper

[a]The age is calculated using 2001 September 13 (UT) as the date of explosion.

[b]Array configuration relevant only for VLA.

NOTE—Stockdale+04 ≡ (Stockdale et al. 2004), Bietenholz+04 ≡ (Bietenholz et al. 2004), Paragi+05 ≡ (Paragi et al. 2005),BB+07 ≡ (Bietenholz & Bartel 2007)

3.3. *Chandra X-ray observations*

We obtained *Chandra* archival data on SN 2001em at 5 epochs between 2004 April and 2016 August. We extracted the *Chandra* spectra, response and ancillary matrices using Chandra Interactive Analysis of Observations software (CIAO; Fruscione et al. 2006), using task `specextractor`. The CIAO version 4.6 along with CALDB version 4.5.9 was used for this purpose. The HEAsoft[2] package Xspec version 12.1 (Arnaud 1996) was used to carry out the spectral analysis.

The spectra were fitted with a thermal bremsstrahlung model and the temperature was fixed at 20 keV. Due to low counts, only 5 channels were averaged and we used maximum likelihood statistics for a Poisson distribution, i.e. the c-statistics[3] (Cash 1979). At the last epoch, we do not detect X-ray emission from the supernova and the upper limit was obtained using a thermal bremsstrahlung model with temperature 20 keV and a column density of 1.5×10^{21} cm^{-2}. Table 2 lists various model fit values and fluxes of the SN at various epochs.

3.4. *XMM-Newton X-ray observations*

XMM-Newton observed SN 2001em on 2006 June for an exposure of around 25 ks. To extract the spectra and response matrices for the *XMM-Newton* data, the Scientific Analysis System (SAS) version 12.0.1 and its standard commands were used. The software `Xspec` was used to carry out the spectral analysis, in a similar way to the *Chandra* analysis. The details are listed in Table 2.

3.5. *Swift-XRT observations*

The X-ray telescope (XRT) onboard *Swift* observed SN 2001em at various epochs during 2008 January to 2016 January. The `xselect` program of HEAsoft package was used to create the spectra and images. Observations closely spaced in time were combined. None of the *Swift*-XRT observations resulted in detection. The 0.3–10.0 keV flux was obtained from the 3σ upper limits on count rates by assuming a thermal plasma of 20 keV and a column density of 1.5×10^{21} cm^{-2}.

In Table 2, we list all X-ray observations.

[2] http://heasarc.gsfc.nasa.gov/docs/software/lheasoft/

[3] The c-statistics minimizes the C value defined as $C = -2\Sigma_i(M_i - D_i + D_i(\ln D_i - \ln M_i))$, where M_i and D_i are defined as the model-predicted and observed counts in each spectral bin i, respectively. Errors in the parameters in c-statistics are estimated as in the χ^2 method, i.e. $\Delta C = C - C_{\rm min}$, where $C_{\rm min}$ is the minimum best-fit C value obtained.

Table 2. X-ray observations of SN 2001em

Date of Observation (UT)	Telescope	Proposal ID	Exposure (ks)	Age[a] (day)	Count rate (cts s^{-1})	Column density (cm^{-2})	Unabs. Flux[b] (erg s^{-1} cm^{-2})
2004 Apr 04	*Chandra*	5306	14.57	934	$(10.55 \pm 0.88) \times 10^{-3}$	$(2.69 \pm 0.59) \times 10^{21}$	$(1.58 \pm 0.13) \times 10^{-13}$
2006 Jun 14	*XMM-Newton*	0405730101	19.70	1735	$(38.49 \pm 5.04) \times 10^{-3}$	$(1.35 \pm 0.73) \times 10^{21}$	$(1.56 \pm 0.23) \times 10^{-13}$
2007 Apr 23	*Chandra*	7606	4.98	2048	$(5.29 \pm 1.10) \times 10^{-3}$	$(2.08 \pm 1.51) \times 10^{21}$	$(7.77 \pm 1.69) \times 10^{-14}$
2008 Jan 03	*Chandra*	9094	4.98	2303	$(3.65 \pm 0.90) \times 10^{-3}$	$(1.71 \pm 1.78) \times 10^{21}$	$(4.84 \pm 1.37) \times 10^{-14}$
2008 Jul 20	*Swift*-XRT	37982001	2.20	2502	$< 5.06 \times 10^{-3}$	1.7×10^{21} (fixed)	$< 3.05 \times 10^{-13}$
2009 Aug 22	*Chandra*	11227	10.05	2900	$(2.96 \pm 0.61) \times 10^{-3}$	$(1.52 \pm 1.29) \times 10^{21}$	$(3.67 \pm 0.81) \times 10^{-14}$
2012 Jan 11	*Swift*-XRT	45809001	0.87	3772	$< 15.9 \times 10^{-3}$	1.5×10^{21} (fixed)	$< 9.62 \times 10^{-13}$
2012 Jun 17	*Swift*-XRT	45809002	1.26	3930	$< 10.8 \times 10^{-3}$	1.5×10^{21} (fixed)	$< 6.53 \times 10^{-13}$
2012 Oct 03–Oct 13	*Swift*-XRT	45809003-004	2.16	4043 ± 5	$< 7.16 \times 10^{-3}$	1.5×10^{21} (fixed)	$< 4.33 \times 10^{-13}$
2013 Jan 08–Jan 10	*Swift*-XRT	45809005-007	3.99	4137 ± 1	$< 3.99 \times 10^{-3}$	1.5×10^{21} (fixed)	$< 2.05 \times 10^{-13}$
2013 Apr 04	*Swift*-XRT	45809008	0.77	4221	$< 15.1 \times 10^{-3}$	1.5×10^{21} (fixed)	$< 9.13 \times 10^{-13}$
2013 Jun 25	*Swift*-XRT	45809009	4.01	4303	$< 5.46 \times 10^{-3}$	1.5×10^{21} (fixed)	$< 3.30 \times 10^{-13}$
2015 Jan 10	*Swift*-XRT	45809010	0.46	4867	$< 24.9 \times 10^{-3}$	1.5×10^{21} (fixed)	$< 1.51 \times 10^{-12}$
2015 Apr 08–Apr 22	*Swift*-XRT	45809011-013	1.04	4962 ± 7	$< 11.2 \times 10^{-3}$	1.5×10^{21} (fixed)	$< 6.77 \times 10^{-13}$
2015 Jun 29–Jul 04	*Swift*-XRT	45809014-015	0.47	5040 ± 2	$< 33.1 \times 10^{-3}$	1.5×10^{21} (fixed)	$< 2.00 \times 10^{-12}$
2016 Jan 06	*Swift*-XRT	45809010	0.20	5228	$< 58.5 \times 10^{-3}$	1.5×10^{21} (fixed)	$< 3.54 \times 10^{-12}$
2016 Aug 19	*Chandra*	18031	14.86	5454	$< 8.10 \times 10^{-4}$	1.5×10^{21} (fixed)	$< 1.45 \times 10^{-14}$

[a] The age is calculated using 2001 September 13 (UT) as the date of explosion.

[b] Unabsorbed flux in 0.3–10 keV energy range.

NOTE—We have fixed the temperature to 20 keV for all observations to derive the SN 2001em flux.

4. MODELING AND RESULTS

4.1. *Visual inspection of radio data*

In Fig. 3, we plot SN 2001em light-curves covering frequencies between 0.4 GHz to 22.5 GHz and near-simultaneous spectra between epochs 873 days to $\sim$ 6870 days. The light curves make a transition from optically thick to optically thin phase at all observed frequencies, with peak of the light curve progressively moving to later times at lower frequencies. At 1.4 GHz, SN 2001em turned on at around 1100 days and peaked at $\sim$ 1700 days. The spectra seem to follow the standard expected evolution until day 2573, as the peak of the spectra move to progressively lower frequencies at later epochs and eventually evolve to the optically thin phase at all observed frequencies, indicating the absorption peak has moved below 1.4 GHz. The peak spectral luminosities at different radio frequencies lie within $(1.1-1.8)\times10^{28}$ erg cm^{-2} s^{-1} Hz^{-1}. This places SN 2001em among the most luminous radio supernovae (Chandra 2018).

The most unexpected features are in the spectra post 5000 days. Since the spectra are at late epochs and the fractional change in the supernova age is only 10% between these two epochs, we combine the Dec 2019 and mid 2020 data. The spectrum declines at low frequencies but starts to rise again at higher frequencies, and then making a second turn at around 15 GHz (Fig. 3). We discuss this feature in the next section (§5).

4.2. *Radio emission models*

Radio emission mainly arises from the forward shock and is synchrotron in nature. We use the self-similar synchrotron emission models developed by Chevalier (1982); Chevalier & Fransson (2017), where the shock radius evolves as power-law in time, i.e. $r \propto t^m$, m is the shock deceleration parameter and is connected to the outer ejecta density profile index n (in $\rho_{\rm ej} \propto r^{-n}$) as $m = (n-3)/(n-s)$. Here s is the index of the power-law density profile in the unshocked CSM, ρ_w, created by the stellar wind of the progenitor star ($\rho_w \propto r^{-s}$). A steady stellar wind is generally assumed for the progenitor wind, i.e. $s = 2$. However, SNe IIn are known to deviate significantly from the steady wind model (Chandra et al. 2012, 2015; Dwarkadas & Gruszko 2012). Therefore, we generalize our model and keep s as a free parameter.

The radio synchrotron emission undergoes suppression, due to free-free absorption (FFA) by the ionised CSM (Chevalier 1982) and/or due to synchrotron self-absorption (SSA) by the same electron population responsible for the radio emission (Chevalier 1998). In a model where FFA is the dominant absorption mechanism, the radio flux density, $F(\nu, t)$, can be expressed as (Chevalier 1982; Weiler et al. 2002)

$$F(\nu,t) = K_1 \left(\frac{\nu}{5\ {\rm GHz}}\right)^{-\alpha} \left(\frac{t}{1000\ {\rm day}}\right)^{-\beta} e^{-\tau_{\rm ffa}(\nu,t)}, \quad (1)$$

where K_1 is a normalization factor whose value is equal to the radio flux density at 5 GHz measured at day 1000 after the explosion. The indices α and β denote the

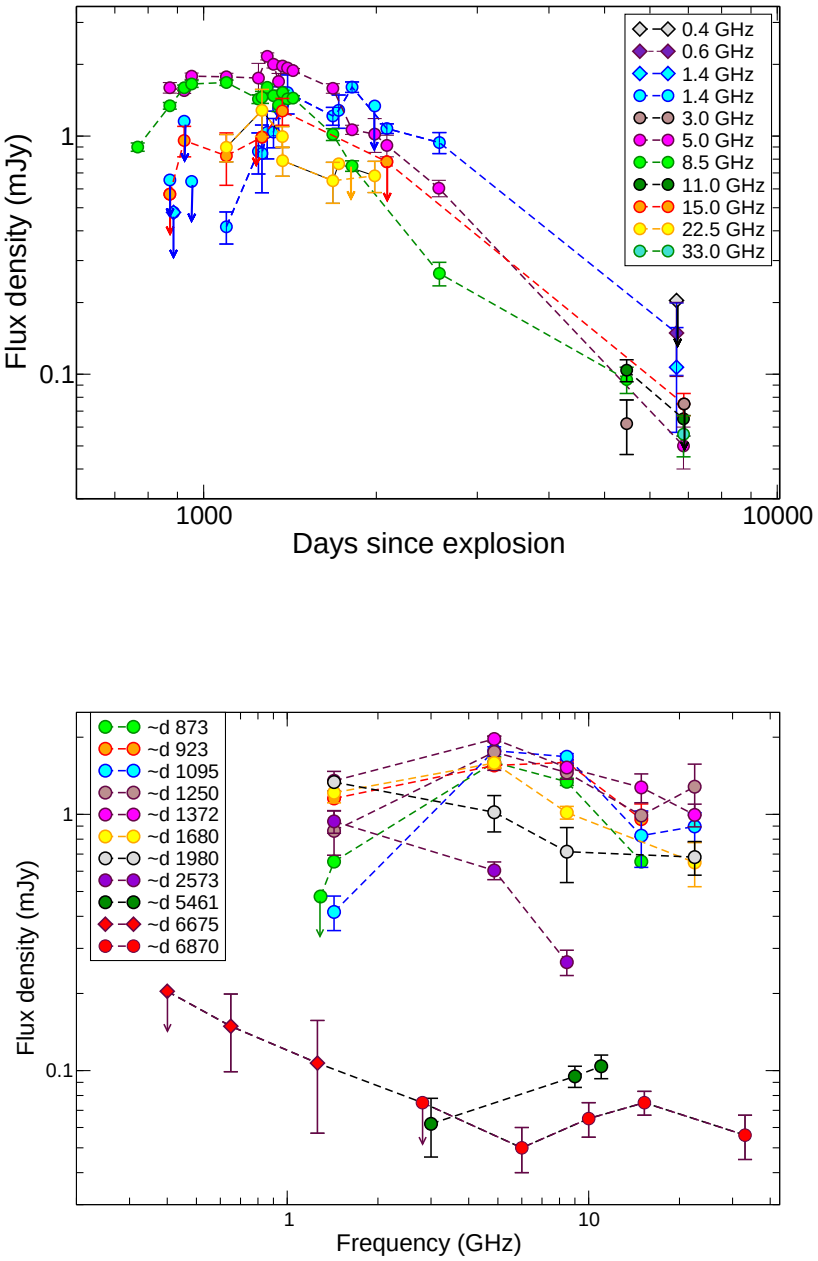


Figure 3. *Top panel:* The radio light curves of SN 2001em at various frequencies. *Bottom panel:* Radio spectra of SN 2001em at various epochs. The last epoch represents spectra at $\sim 6000 \pm 500$ days. In both the plots, the circles represent VLA data and the diamonds represent GMRT data.

spectral and temporal evolution in the optically thin phase, respectively. The radio spectral index α is related to the electron energy index p (in $N(E)dE \propto E^{-p}dE$) as $\alpha = (p-1)/2$. The assumptions that the energy density in the particles and the magnetic field are proportional to the postshock energy density lead to the parameter

$\beta = (3+\alpha)(ms+2-2m)/2-3m$. Here $\tau_{\rm ffa}$ is the FFA optical depth due to ionized CSM external to the emitting material, and can be written as

$$\tau_{\rm ffa}(\nu,t) = K_2 \left(\frac{\nu}{5\ {\rm GHz}}\right)^{-2.1} \left(\frac{t}{1000\ {\rm day}}\right)^{-\delta}, \quad (2)$$

where K_2 denotes the free-free optical depth at 5 GHz measured at day 1000 after the explosion. As the shock wave expands, the optical depth decreases with time as $t^{-\delta}$, where δ is related to shock deceleration parameter m as $\delta = m(2s-1)$.

The high densities in SNe IIn indicate that FFA is likely to be the dominant absorption mechanism (Chevalier 1998). However, since SN 2001em initially exploded as a Type Ib/c supernova, SSA could be important and we account for this possibility. The radio flux density for the SSA dominated synchrotron emission can be written as (Chevalier 1998):

$$F(\nu,t) = K_1 \left(\frac{\nu}{5\ {\rm GHz}}\right)^{2.5} \left(\frac{t}{1000\ {\rm day}}\right)^{\beta'} (1-e^{-\tau_{\rm ssa}(\nu,t)}), \quad (3)$$

where the optical depth is characterised by SSA due to the relativistic electrons at the forward shock. The SSA optical depth τ_{ssa} is given by

$$\tau_{\rm ssa}(\nu,t) = K' \left(\frac{\nu}{5\ {\rm GHz}}\right)^{-(\alpha+2.5)} \left(\frac{t}{1000\ {\rm day}}\right)^{-(\beta'+\beta)}. \quad (4)$$

K_1 and K' are the flux density and optical depth normalisation factors similar to the case of FFA. The flux density in the optically thick and thin phases behave as $\nu^{2.5}$ and $\nu^{-\alpha}$, respectively. Here $t^{-\beta}$ is the time evolution of the flux density in the optically thin phase, and $t^{\beta'}$ for the optically thick phase. The exact form of β and β' depend upon the scalings of magnetic field, B, and electron energy density (Chevalier 1996). If we assume that the magnetic energy density and relativistic electron energy density scale with post shock energy density (model 1 of Chevalier 1996), then the optically thick light curve, $F_\nu(t) \propto R^2 B^{-1/2}$, leads to $\beta' = 2m+0.5$ and $\beta = (p+5-6m)/2$ for $s=2$.

In the high density environment of SNe IIn, the reverse shock becomes radiative and a cool dense shell is likely to form between the forward and reverse shocks because of the higher density of the CSM. In this case a fraction of the cool gas mixed into the synchrotron emitting region can cause internal FFA. Weiler et al. (1990) developed a formulation for internal FFA to explain the radio data of SN 1986J. The early radio emission is described by the escape probability from a clumpy region. Chandra et al. (2012) showed that a modest amount of cool gas mixed into the synchrotron emitting gas was sufficient to explain the absorption in SN 2006jd radio emission. The internal FFA model is described as (Weiler et al. 1990):

$$F(\nu,t) = K_1 \left(\frac{\nu}{5\,{\rm GHz}}\right)^{-\alpha} \left(\frac{t}{1000\,{\rm day}}\right)^{-\beta} \left(\frac{1-\exp(-\tau_{\rm intFFA}(\nu,t))}{\tau_{\rm intFFA}(\nu,t)}\right),$$

$$\tau_{\rm intFFA}(\nu,t) = K_3 \left(\frac{\nu}{5\,{\rm GHz}}\right)^{-2.1} \left(\frac{t}{1000\,{\rm day}}\right)^{-\delta'}, \qquad (5)$$

where we allow $s \neq 2$; α and β are expressed as above for the FFA model. Weiler et al. (1990) have assumed that the internal absorbing gas is homologously expanding with density $n \propto R^{-3} \propto t^{-3m}$, which will lead to $\tau_{\rm intFFA} \propto n^2 R \propto t^{-5m}$, or $\delta' = -5m$. However, this may not be the case and the prevailing conditions are unknown. We account for other possibilities for δ' and allow it to be a free parameter.

To apply the CSM interaction model to SN 2001em radio data, we consider the same sequence of events as given by Chugai & Chevalier (2006). SN 2001em lost all of the H-envelope before the explosion and exploded as a stripped envelope supernova. However, the H-rich material did not have enough time to be completely dispersed into the interstellar medium and was located close enough so that the ejecta were able to catch up with this H-shell, and the subsequent interaction produced radio and X-ray emission and broad Hα emission. The H-envelope may have been emitted during a red supergiant phase with a wind speed of $v_{\rm w} \sim 10\,{\rm km\,s^{-1}}$, and got accelerated by the fast W-R winds to $30 - 50\,{\rm km\,s^{-1}}$.

Several phases of evolution can be identified, depending on the circumstellar density profile, which is illustrated in Fig. 4. Initially (Phase - 1), the outer supernova ejecta interact with the fast wind of the progenitor star, followed by interaction with shocked wind. This phase of low density interaction was missed in radio and X-ray observations of SN 2001em. Next is a transition between Phase - 1 and Phase -2 during which the increasing pressure of the shocked ejecta drives a shock front into the dense shell (Chevalier & Liang 1989). The increasing pressure is accompanied by increasing X-ray and radio emission. In Phase - 2, the emission is mainly from the shell interaction. This emission drops when the shock front comes out of the dense region and eventually the interaction with the outer circumstellar medium dominates the emission (Phase - 3). The transition may occur over several dynamical timescales during which the shock velocity is roughly constant (van Marle et al. 2010) or might accelerate (Harris et al. 2016).

4.3. *Model fits to radio data*

We now carry out detailed fits to the radio data. We use Markov chain Monte Carlo (MCMC) fitting using the Python package emcee (Foreman-Mackey et al. 2013). We choose 200 walkers, 1000 steps, and flat priors on all of the parameters. We obtain best-fit values (at 68% confidence interval, i.e., 1σ).

SN 2001em lacks early radio and X-ray data and its Phase–1 was completely missed. We need to fit for Phase–2 and Phase–3. Since the data are sparse at later epochs, it is not clear when the Phase–2 ended, although towards the end of this section we try to answer this question. We start with global fits using the FFA and the SSA models to all the data. We list the best fit parameters of FFA and SSA models in columns 1 and 2 of Table 3, respectively. We note that none of the models are a

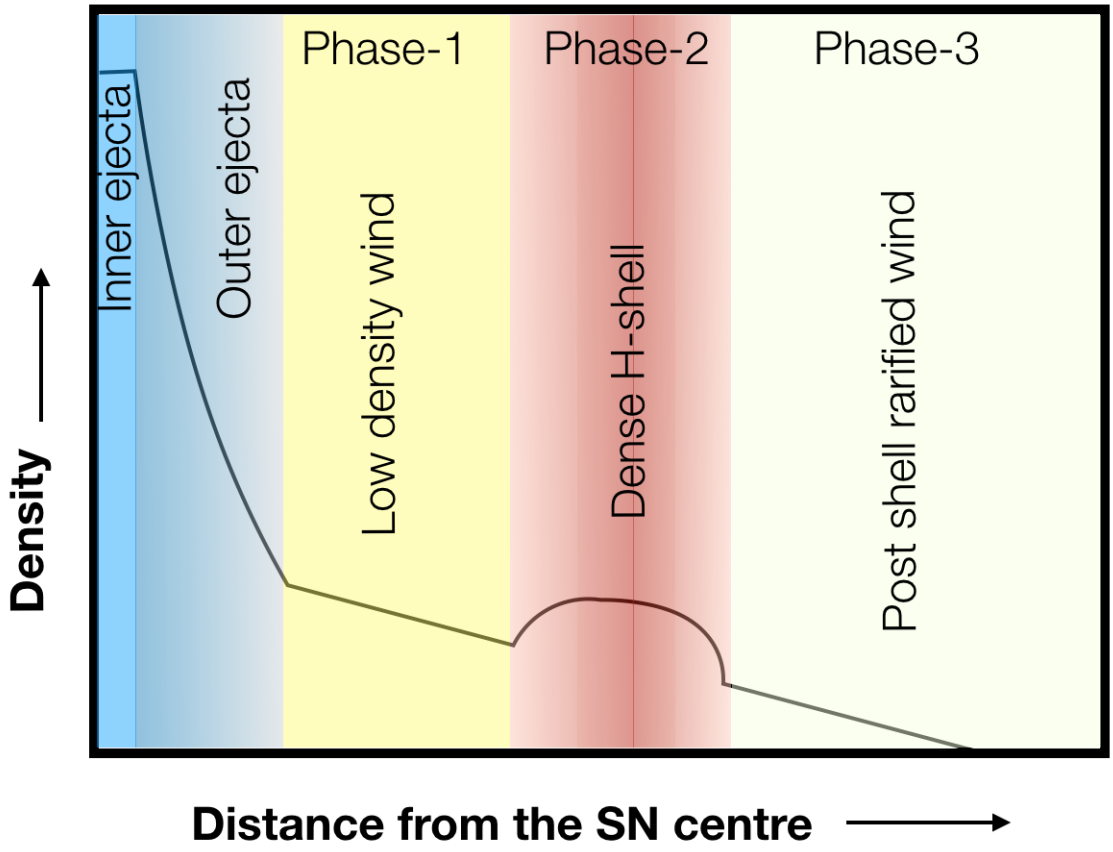


Figure 4. Cartoon diagram of various ejecta and wind density profiles.

good fit to the data with large values of reduced Chi-square (χ^2_ν). In addition, both models give best-fit $\alpha < 0.5$, suggesting a hard electron energy index $p < 2$, which is observationally not the case (Fig. 3). While the FFA fit is slightly better, the derived best values of α, β and δ result in $m \approx 1.46$, which is not consistent with the hydrodynamic model.

One can independently estimate the significance of SSA model based on the velocity of the ejecta at the SSA peak (Chevalier & Fransson 2017, and references therein). The 8.5 GHz peak comes around day 1000 with a peak flux density of ~ 1.7 mJy. Using Eq. 59 of Chevalier & Fransson (2017), we obtain the size deduced from the SSA model as $\sim 1\times10^{16}$ cm, suggesting the velocity $\sim 1000\,\mathrm{km\,s^{-1}}$ at 1000 days. This is quite small for a SN shock and also smaller than the ejecta velocity of $> 1800\,\mathrm{km\,s^{-1}}$ around day 970 obtained from the Hα FWHM (Soderberg et al. 2004), suggesting SSA is not the dominant radio absorption.

The internal FFA model of Weiler et al. (1990) is a better representation of the data with improved fit statistics (column 3 of Table 3). As in the case of SN 1986J, we now account for the possibility that the radio emission is absorbed by both external as well as internal thermal absorbers. We note that internal+external FFA gives better fits (column 4 in Table 3). The derived value of s for this model is $s = 1.80 \pm 0.26$. This

Table 3. Best fit parameters for the FFA & SSA models to the radio data

FFA	SSA	Int. FFA	Ext.+Int. FFA	Ext.+Int. FFA ($s = 2$)
(1)	(2)	(3)	(4)	(5)
$K_1 = 2.43^{+0.11}_{-0.10}$ $K_2 = 0.41^{+0.04}_{-0.03}$ $\alpha = 0.41^{+0.03}_{-0.03}$ $\beta = 1.49^{+0.07}_{-0.07}$ $\delta = 7.28^{+0.30}_{-0.29}$.	$K_1 = 3.11^{+0.20}_{-0.19}$ $K' = 0.75^{+0.08}_{-0.07}$ $\alpha = 0.40^{+0.03}_{-0.03}$ $\beta = 1.45^{+0.07}_{-0.07}$ $\beta' = 8.39^{+0.31}_{-0.31}$	$K_1 = 2.79^{+0.16}_{-0.14}$ $K_3 = 1.37^{+0.16}_{-0.14}$ $\alpha = 0.48^{+0.04}_{-0.04}$ $\beta = 1.68^{+0.09}_{-0.09}$ $\delta' = 7.04^{+0.33}_{-0.33}$	$K_1 = 3.07^{+0.16}_{-0.15}$ $K_2 = 0.13^{+0.02}_{-0.02}$ $K_3 = 0.68^{+0.13}_{-0.11}$ $\alpha = 0.69^{+0.05}_{-0.05}$ $\beta = 1.63^{+0.08}_{-0.08}$ $\delta = 1.60^{+0.16}_{-0.08}$ $\delta' = 10.02^{+0.58}_{-0.64}$	$K_1 = 3.00^{+0.17}_{-0.16}$ $K_2 = 0.15^{+0.02}_{-0.02}$ $K_3 = 0.61^{+0.15}_{-0.13}$ $\alpha = 0.65^{+0.05}_{-0.05}$ $\delta = 2.02^{+0.07}_{-0.07}$ $\delta' = 10.48^{+0.89}_{-0.81}$
$\chi^2_\nu = 3.27$ *d.o.f.*=56	$\chi^2_\nu = 3.28$ *d.o.f.*=60	$\chi^2_\nu = 2.89$ *d.o.f.*=56	$\chi^2_\nu = 2.19$ *d.o.f.*=54	$\chi^2_\nu = 2.21$ *d.o.f.*=55

value is very close to $s = 2$, so we again fit the internal+external FFA model, but fixing $s = 2$, so that $\beta = 3+\alpha-\delta$. We also exclude data points from day 5460 onwards as they appear to arise from a different component (§4.1). This model (column 5 in Table 3) provides a good fit to the data amongst all the models considered. This model results in $m = 0.67 \pm 0.08$, probably indicating deceleration after the shock entered the H-shell. Figure 5 shows the corner plot with the results of the MCMC fit for this model. The parameters are well constrained with internal absorption being the dominant absorption mechanism. In Fig. 6, we plot the best fit light curves and spectra.

We note that the reduced χ^2_ν is still large. This is probably because the evolution is not smooth and there is detailed structure in the radio light curves. The contribution to the χ^2 is more from the radio fluctuations rather than the model fits. The contribution of internal absorption is 4 times higher than the FFA. This means that the radio emission is arising from a shocked region containing clumpy gas. The clumpiness could come from hydrodynamic instabilities at the contact discontinuity or from clumpiness in the ejecta or the surrounding region.

In Fig. 6, we plot light curves and spectra along with the best fit model. For the late time spectrum, we combine the high frequency VLA data around day 6870 with the low frequency upgraded GMRT data on day 6675 and plot them at an average epoch of $\sim$ 6772 day. The model fits adequately represent the light curves at early times and capture the overall evolution rather well. However, the fits to the spectra are not as good as the light curves. There are two points to note: on day 870, the spectrum seems to suggest a peak at frequencies lower than predicted by the model. This could mean the actual density is lower than that predicted by the model. One explanation is if the shock entered not so long ago in the dense shell, and the shock is still catching up to the high density region within the shell, which probably is somewhere at the center part (Fig. 4). However, the spectrum consists of only three measurements and fluctuations might simply be caused by the clumpy density profile.

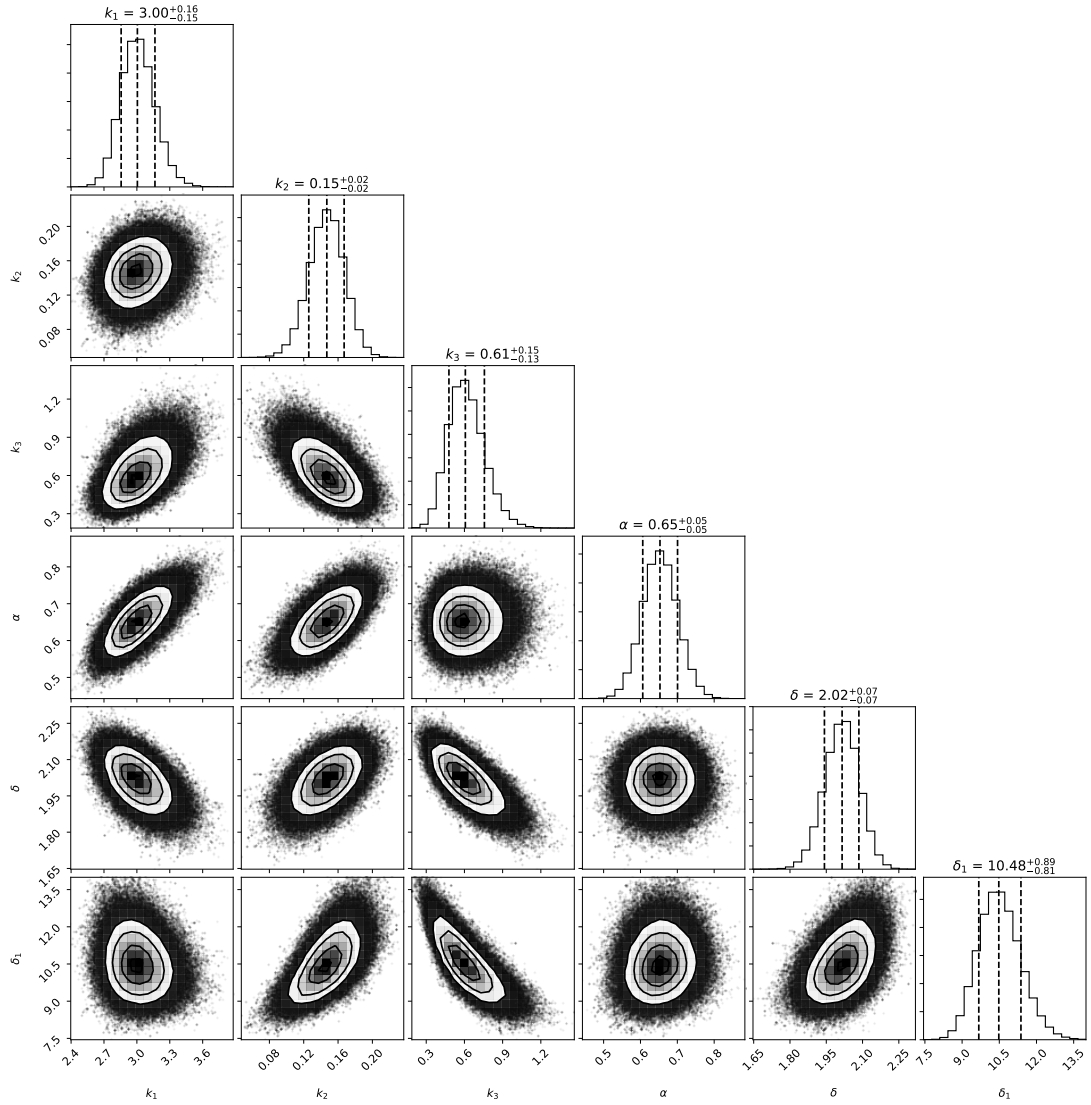


Figure 5. Corner plot with the MCMC fit to the internal+external model of the radio emission with $s = 2$ for SN 2001em .

There is one early data point on day 764 at 8.46 GHz which is consistent with the overall light curve model (Fig. 6).

The most interesting trend is seen at the latest near-simultaneous spectra on day 5460 and 6772 (Fig. 6). While the model predicts an optically thin spectrum at all frequencies, the observed spectrum turns over at around ≥ 3 GHz and becomes optically thick. The X-ray observations at this epoch result in an upper limit, which is not constraining. The behavior can be explained if there is a central absorbed component, which is unveiled as the absorption of the inner source and the flux of the outer source decline. The lower than expected optically thin spectrum at lower frequencies could be an indication of the forward shock moving in a low density medium. This can also explain the spectrum on day 2500. The 8.5 GHz flux is smaller than expected from the best fit model, which could be an indication that

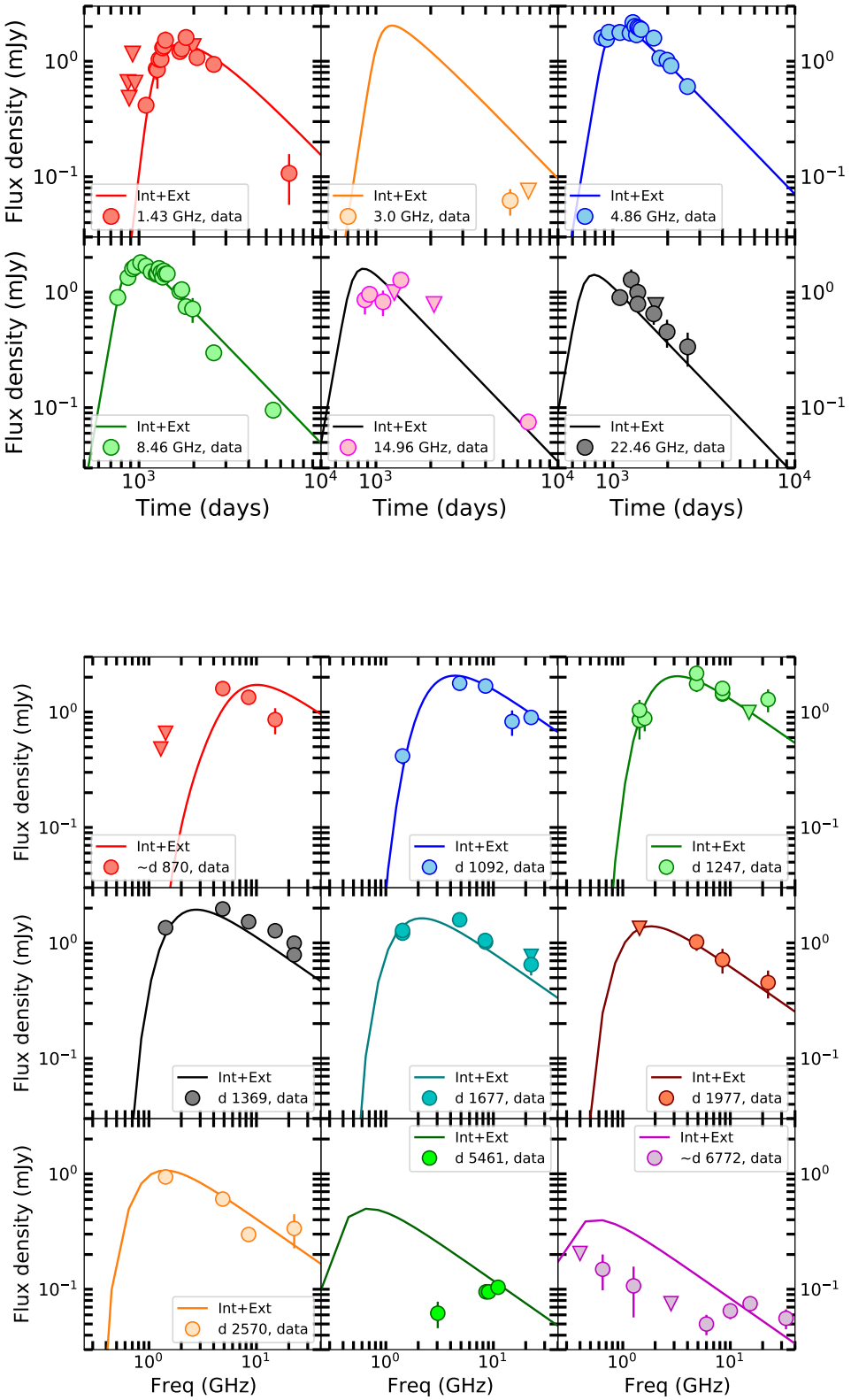


Figure 6. Radio light curves (top panel) and spectra of SN 2001em fit with the internal+external FFA model. The model fits the data well between 1000 – 2500 days.

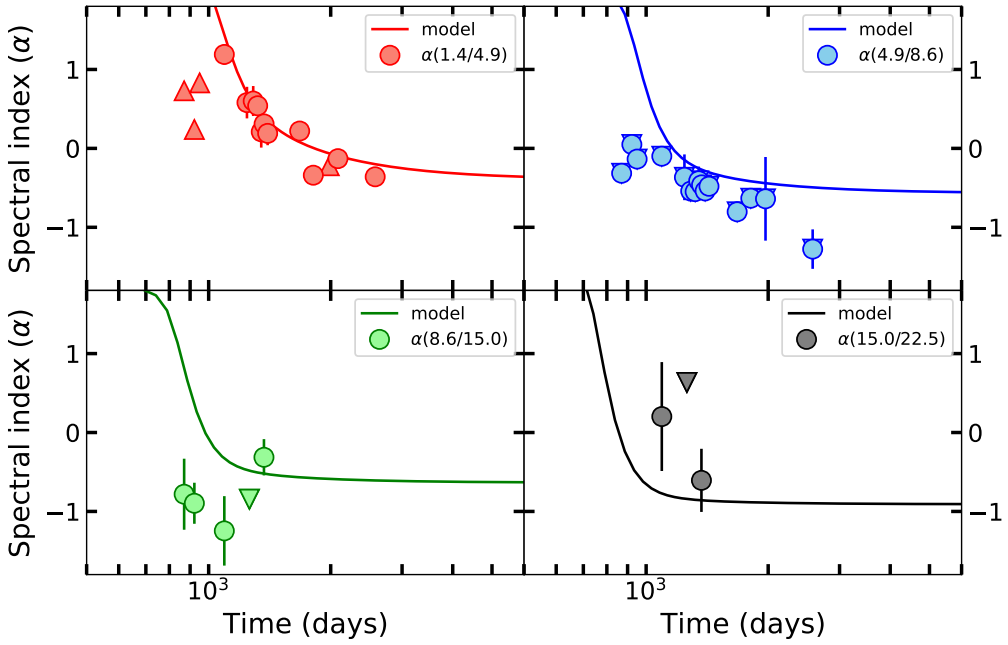


Figure 7. Spectral index at different adjacent frequencies. The spectral index moves from positive to negative values indicating a transition from optically thick phase to optically thin phase. The thick solid lines are the best fit internal+external absorption models. The triangles are limits, in the direction that the triangle is pointing.

the shock is leaving the dense shell and moving into the steeply decreasing density, consistent with the X-ray data. The higher flux at 22.5 GHz component could then be coming from the central absorbed component, seen clearly from day 5461 onwards.

In Fig. 7, we plot the spectral indices (α; in $F(\nu) \propto \nu^{\alpha}$) between the observed adjacent frequencies. The values of α are mostly negative after around 1000 days indicating an optically thin medium, except between 1.4 and 4.9 GHz. The values of α between these two frequencies are positive up to the first 3.5 years before making a transition to the optically thin phase. We derive the model spectral indices from the best fit parameters and overplot them in Fig. 7. They seem to represent the data reasonably well, giving support to the internal+external model. We compare the spectral evolution for SN 2001em to that of SN 1986J, which was also explained by the internal+external absorption model. The resemblance is striking (Fig. 8), suggesting that the presence of a cool-dense shell or clumps in the case of dense interaction is common and contributes towards extra absorption of radio emission as internal FFA.

4.4. *Mass-loss rate*

We can now attempt to constrain the mass-loss rate from the radio data. Weiler et al. (2002) and Chevalier & Fransson (2017) derived the mass-loss rate formula

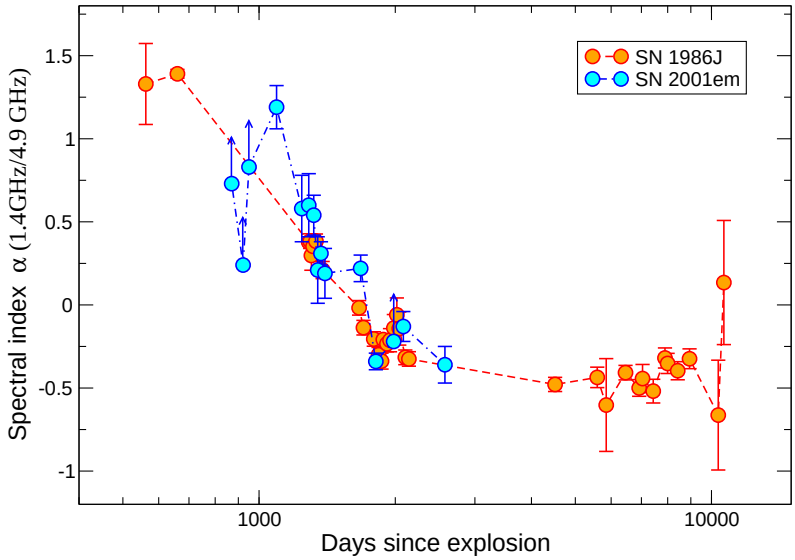


Figure 8. The spectral index evolution for SN 2001em and SN 1986J between 1.4 and 4.9 GHz frequencies. The SN 2001em spectral evolution approximately follows that of SN 1986J. The arrows represent the limits in the direction they are pointing.

considering multiple absorption components:

$$\left(\frac{\dot{M}_{-3}}{v_{w1}}\right) = 7.5\times10^{-2}\left(\frac{\langle\tau_{\rm eff}\rangle}{1+[n({\rm He})/n({\rm H})]}\right)^{0.5}\left(\frac{\nu}{\rm GHz}\right)^{1.06}\left(\frac{T}{10^4\,{\rm K}}\right)^{0.67}\left(\frac{v_s}{10^4\,{\rm km\,s^{-1}}}\right)^{1.5}\left(\frac{t}{1000\,{\rm d}}\right)^{1.5}. \quad (6)$$

Here, $\langle\tau_{\rm eff}\rangle$ is the effective optical depth considering all absorption effects. We need the velocity of the radio emitting shock v_s and T, the CSM temperature. We assume $T \sim 10^4$ K. To estimate the velocity, we note that the Hα emission had a FWHM of $\sim$1800 km s^{-1}. As the supernova at the time of explosion was a stripped envelope supernova, one expects Hα to arise from the shocked CSM. In such a case the Hα width reflects the lower limit to the forward shock velocity, the actual velocity will be closer to the base of the Hα profile. However, it gives the order of the velocity. From X-ray observations, the temperature is $\geq$ 15 keV, corresponding to a velocity $>$ 3500 km s^{-1} velocity. From VLBI observations, Schinzel et al. (2008) put an upper limit to the expansion velocity of 6000 km s^{-1}. Bietenholz & Bartel (2005) obtained an expansion velocity of 5800 ± 10000 km s^{-1} in their measurements on day 1770, which is consistent with an expansion velocity from zero to 10^4 km s^{-1}. In the case of SN 2014C, *NuSTAR* data were available and the temperature was found to be at $\sim$ 20 keV (Margutti et al. 2017). Similarly for SN 2010jl, the *NuSTAR* measurements revealed the forward shock temperature to be $\sim$ 18 keV (Chandra et al. 2015), corresponding to a velocity of $\sim$ 3700 km s^{-1}. In case of SN 1996cr, which is also interacting with

a dense shell, Dwarkadas et al. (2010) found the X-ray emitting shock to be moving with 4740 km s^{-1}. VLBI observations of SN 1986J showed an expansion speed around 1000 days to be 5700 km s^{-1}(Bietenholz et al. 2004). We thus adopt 4000 km s^{-1} to be an expansion speed for SN 2001em.

Our best fit model predicts mass-loss rates of $(5.2 - 0.9) \times 10^{-3}\, M_{\odot}\, \mathrm{yr}^{-1}$ during epochs 170 to 370 years before explosion, for a wind speed of 50 km s^{-1}.

4.5. *X-ray analysis*

The X-ray data cover epochs ranging from day 934 to day 5454. While the radio data are sampled more densely between day 764 and day 2575, the X-ray data have sparser coverage up to day 1735 and have better coverage afterwards (Fig. 9). However, none of the *Swift*-XRT observations (which were taken at later epochs) resulted in a detection and the upper limits are not constraining. The last epoch *Chandra* observation on day 5464 also resulted in an upper limit. The highest X-ray flux corresponds to an unabsorbed $0.3 - 10$ keV X-ray luminosity $L_{\mathrm{Xray}} = 1.25 \times 10^{41}$ erg s^{-1}, placing it among the brightest X-ray supernovae (Chandra 2018).

The *XMM*-Newton data at day ~ 1735 are the best dataset to constrain the temperature. We fit the data with an absorbed thermal bremsstrahlung model. We find that the temperature in our model is not well constrained. Within the sensitivity of the *XMM*-Newton energy range, it is not bounded by an upper limit. The lower bound is 13 keV. Thus we fix the temperature to 20 keV to carry out the X-ray analysis. Pooley & Lewin (2004) found a temperature of 80 keV, but due to the limited *Chandra* band it is not possible to constrain the temperature to these high values. Our value is assumed to be like that found in SN 2014C by Margutti et al. (2017), who found the plasma temperature producing X-rays to be ~ 20 keV using *NuSTAR* observations.

The temporal evolution between days 934 and 1735 is defined by 2 data points, giving $F_{\mathrm{Xray}}(t) \propto t^{0.05}$ up to around the *XMM*-Newton epoch, i.e. day 1735. One possibility is that the X-ray flux remained constant between these two epochs and then started to fall rapidly afterwards. However, a peak between these two epochs is plausible. We plot one such possibility in Fig. 9. Due to the lack of early data points, it is not possible to further constrain the evolution.

The light curve falls steeply after day 1735, steepening to $F_{\mathrm{Xray}}(t) \propto t^{-3.12 \pm 0.66}$. Such an evolution at late time is possible if the forward shock wave moved out of the shell and into lower density gas. In the radio spectrum on ~ 2500 d, the 8.5 GHz data point is much below the standard model with $s = 2$, consistent with the X-ray prediction. There is an increase in the 22 GHz flux density, which can be explained if this component is coming from a central absorbed component, causing the flux density to rise.

Since the temperature of the emitting region is higher than can be measured in the 0.3–10 keV bandpass of the X-ray detectors used, our values represent the spectral

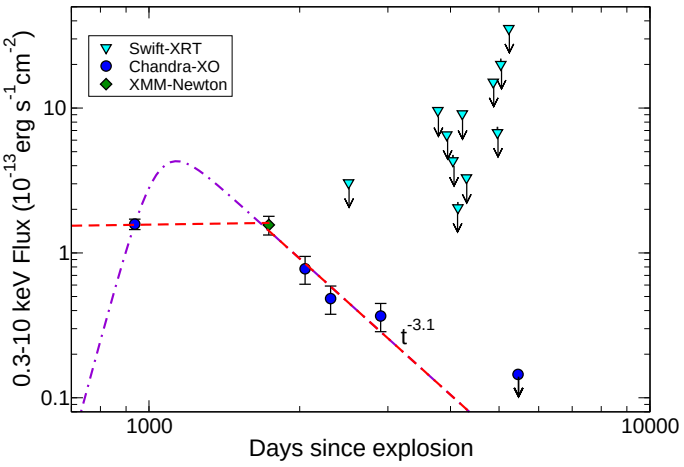


Figure 9. The 0.3–10.0 keV X-ray light curve of SN 2001em. Due to only two data points between 934 and 1735 days, the X-ray evolution is poorly constrained before day 1735, except that the X-ray peak lies somewhere between 934 and 1735 days. One possibility is that the X-ray flux remained constant between these two epochs (red dashed line) and then started to fall rapidly. However, various evolutions are possible with a peak between these two epochs. The purple dot-dashed line shows one such possibility for illustrative purposes. The evolution after 1735 days is well constrained, with the flux declining as $F_{\rm Xray}(t) \propto t^{-3.1}$.
.

flux rather than the total X-ray flux. For bremsstrahlung emission and slow cooling, the X-ray spectral luminosity can be written as $L_{\rm Xray} \propto n^2 V/T^{1/2}$, where V is the emitting volume (Chandra et al. 2012). As $R \propto t^{-m}$ and $n \propto R^{-s}$, this implies $L_{\rm Xray} \propto t^{2m(1-s)+1}$. A value of $s \sim 3$ can reproduce the steeper decline.

Between day 934 and day 2900, the column density evolves from $\sim (2.7 \pm 0.6) \times 10^{21}\,{\rm cm}^{-2}$ to $(\sim 1.3 \pm 0.7) \times 10^{21}\,{\rm cm}^{-2}$ (Fig. 10D). Afterwards we do not have sensitive measurements to constrain the column density. While the error-bars are large, we attempt to fit a power law to the evolution of column-density and it fits best with an index of -0.71 ± 0.23 (Fig. 10D). Thus, there is evidence for evolution of the column density to a value higher than the Galactic column density $N_H = 6 \times 10^{20}{\rm cm}^{-2}$(Spitzer & Arny 1978), corresponding to the reddening toward SN 2001em, $E(B-V) = 0.1$ (Schlegel et al. 1998).

4.6. *Origin of X-ray emission*

A critical question is to find the origin of X-ray emission. Chugai & Chevalier (2006) modelled the origin of the radio and X-ray emission of SN 2001em to be an 80 keV region produced by a 5500 km s^{-1} reverse shock. However, their modelling had two issues: 1) the velocity of the forward shock was assumed to be 1800 km s^{-1} based on Hα measurements (Soderberg et al. 2004) and, 2) X-ray emitting plasma was considered to have a temperature of 80 keV based on the results of Pooley & Lewin (2004). We note that the speed of 1800 km s^{-1} represents the FWHM of the

Hα profile which is likely to be a lower limit on the forward shock velocity and, as we argue above (§4.4), the forward shock velocity is $\sim 4000\,\mathrm{km\,s^{-1}}$. The shock temperature of 80 keV was measured from *Chandra* observations with a limited 0.3–10 keV band, which is not sensitive to such high temperatures. As discussed above, more robust temperature measurements have been done for a couple of supernovae in a combined *XMM*-Newton and *NuSTAR* spectral analysis covering an energy range 0.3–80 keV.

The forward shock origin of X-ray emission is further supported by two arguments. In supernovae interacting with dense medium, it is likely that the reverse shock becomes radiative and a cool dense shell forms. Our radio modeling gives evidence of the formation of a cool dense shell, hence that the reverse shock is radiative. We estimate the cooling time for reverse as well as forward shocks for $n = 9$. For the mass-loss rates estimates at ages 773 to 1670 days (§4.4), the ratio of cooling time to expansion time is ≤ 1 for most of the period for the reverse shock, whereas, for forward shock it is around 20–200. This further confirms that, while the reverse shock is radiative, the forward shock is adiabatic. Radiative cooling is more important at the reverse shock and the cool dense shell is likely to absorb much of the X-rays emanating from the reverse shock.

We find that the column density is marginally evolving and there is an excess of column density of $\sim (2.1 - 0.7) \times 10^{21}\,\mathrm{cm^{-2}}$. Since the X-ray emission is coming from the forward shock, this column density represents the column density of the CSM. The evolution of CSM column density means that CSM was not completely ionized between the first two X-ray epochs and photoabsorption is important. Chevalier & Irwin (2012) have estimated that if a supernova is in the cooling regime, a 10,000 $\mathrm{km\,s^{-1}}$ shock wave is capable of completely ionizing the surrounding medium, but a 5000 $\mathrm{km\,s^{-1}}$ shock wave is not. The state of ionization in the circumstellar gas is characterized by the value of the ionization parameter ζ. For a hydrogen helium plasma:

$$\zeta \equiv \frac{L_{CS}}{r^2 n} = 42 \left(\frac{L_{\rm CS}}{10^{41}\,\mathrm{erg\,s^{-1}}} \right) \left(\frac{\dot{M}_{-3}}{v_{w1}} \right)^{-1} . \tag{7}$$

We estimate this value for the epochs at which we have estimated the mass-loss rate from radio data. During these epochs, the X-ray luminosity is nearly constant and the parameter ζ varies between $\sim 50 - 200$. It is a regime where the CNO elements may be completely ionized, but Fe is not (Hatchett et al. 1976). Hence the evolving column density can be explained by not fully-ionized CSM plasma.

Our radio measurements imply a CSM column density of $(\mathrm{a\,few}) \times 10^{22}\,\mathrm{cm^{-2}}$, which is nearly an order of magnitude larger than our best fit X-ray measurements. This trend has been seen in other supernovae as well, and has been attributed to the asymmetric nature of the CSM and/or ejecta (Chandra et al. 2012). An asymmetrical density distribution is a natural outcome of the common envelope scenario. Schrøder

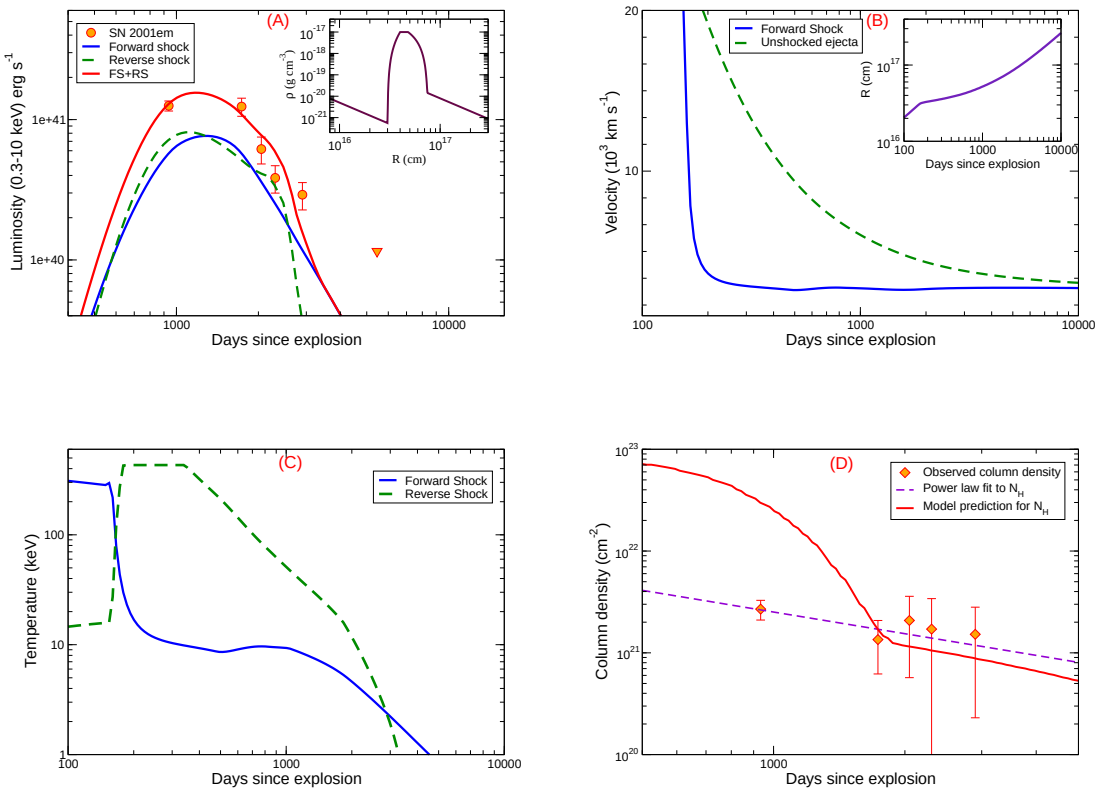


Figure 10. Evolution of X-ray luminosity, expansion velocities and shock temperature in the CS interaction model. Panel *A* shows the X-ray luminosity (*red* line) composed of the emission from the forward shock (*blue solid* line) and reverse shock (*green dashed*) with the overplotted observational data; the *triangle* symbol indicates an upper limit. The inset shows the CS density distribution. Panel *B* shows the velocity of the thin dense shell (*blue solid* line) and the maximal velocity of unshocked ejecta (*dotted*). The radius of the thin shell is shown in the inset. Panel *C* shows the temperature in the forward shock (*blue solid* line) and the reverse shock (*dotted*). Panel *D* shows the best fit X-ray column densities. The evolution is consistent with a power law index of -0.71 ± 0.23. Model fit to N_H is for a fiducial value of the outer density wind profile of $\dot{M}/u_w = 10^{15}\,\mathrm{g\,cm^{-2}}$.

et al. (2020) have carried out hydrodynamic modeling of binary coalescence and found a toroidal distribution of the extended CSM in the binary's equatorial plane.

Due to the low absorption in X-ray and radio emission, Chugai & Chevalier (2006) invoked clumpiness in the absorption, but emission by a smooth CS shell. As ejecta enter into the shell, clumps get fragmented and mixed in the forward shock depositing their full energy to the shock. In this model, absorption is dominated by the clumpy medium but the emission is dominated by the smooth shocked medium. This model predicts a soft component absorbed and reprocessed into optical/UV, in addition to a hard component from the hot forward shock. The lack of data in these bands does not allow us to test this possibility.

We carried out detailed modelling of the X-ray emission following the recipe of Chugai & Chevalier (2006), but with modest revision. The original Chugai & Cheva-

lier (2006) model treats the CS interaction in the thin shell approximation. The density profile of the freely expanding ejecta is an inner flat region outside of which there is a steep power law, r^{-9}. The thermal state of shocked gas in the forward and reverse shocks is described taking into account adiabatic and radiative cooling in the energy equation with volumes of post-shock gas specified by the relative width $\Delta R/R = 0.2$ and 0.1 for the forward and reverse shocks, respectively. The SN ejecta of the former model is set by a mass of $2-3M_\odot$ and a kinetic energy of 1.6×10^{51} erg. The CSM is composed of the inner rarefied WR wind and the outer RSG wind with the massive dense CS shell ($M\sim2-3M_\odot$) at the radius of $(5-7)\times10^{16}$ cm. The CS shell should be clumpy in order to avoid strong absorption of X-rays with an energy of $\lesssim 1$ keV from the reverse shock; the required occultation optical depth is $0.5-1$ (Chugai & Chevalier 2006).

The moderately modified model we use here (Fig. 10) is specified by the ejecta mass of $3M_\odot$, energy of 10^{51} erg, the CS shell ($3M_\odot$) at the distance of $(4-5)\times10^{16}$ cm and the similar inner and outer winds. The model predicts a significant contribution from both forward and reverse shocks, and fits the data satisfactorily (Fig. 10A). The model gas temperature of the reverse shock on day 1735 is 20 keV (Fig. 10C). However, both reverse and forward shocks are adiabatic at $t < 2700$ d. Later on the reverse shock becomes radiative, which is marked by the rapid temperature fall (Fig. 10C). The adiabaticity is in contrast to the analytical analysis and modeling of the radio data. The predicted column density at early epochs ≤ 1600 days is higher than the observed one (Fig. 10D). However, this issue may be resolved taking into account asymmetry and/or the clumpy structure of the CS shell, in which case the Hα emission originates from the shocked clumps with efficient cooling.

Summing up, in the modified Chugai & Chevalier (2006) model, the X-ray emission arises from the contribution of both reverse and forward shocks driven by the ejecta interaction with the massive clumpy CS shell, while the Hα emission is related to the shocked clumps of this CS shell. However, this model should be considered as a simplified description of the three-dimensional (3-D) situation. In the scenario of a clumpy shell the Hα width is related to cloud shocks, whereas the speed of the interclump forward shock should significantly exceed 2000 km s^{-1}, and generally be consistent with the 4000 km s^{-1} supported by other observational constraints. A better handle on multi-waveband data and a more realistic model with 3D-hydrodynamics with a proper treatment of thermal and radiation processes in a multi-phase medium are needed, but are out of the scope of this paper.

5. DISCUSSION

5.1. *Phases of circumstellar interaction in SN 2001em*

We have carried out a comprehensive analysis of radio and X-ray emission from SN 2001em. We have qualitatively defined the evolution in three phases. We did not catch the interaction in Phase - 1 because by the time the radio and X-ray

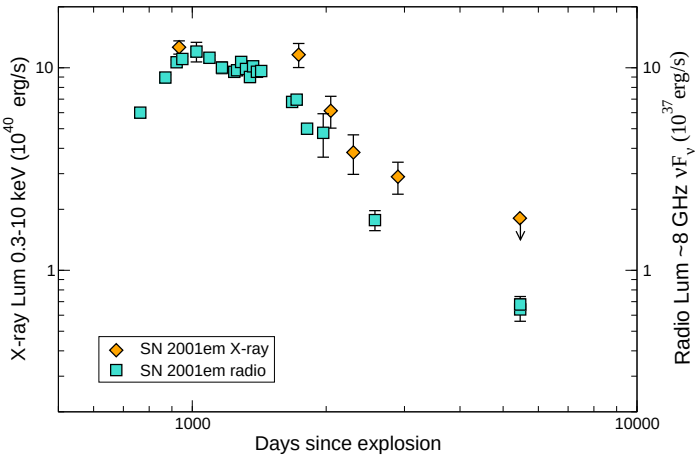


Figure 11. The νF_ν plot for SN 2001em X-ray (0.3–10 keV) and radio data at 8.5 GHz. The left side y-axis is labelled for the X-ray flux and the right side y-axis is labelled for the radio flux.

observations commenced, the supernova ejecta were already interacting with the shell. Our model favours a forward shock origin for the X-ray emission. The modified Chugai & Chevalier (2006) model suggests X-ray emission having a contribution from both shocks, but requires both shocks to be adiabatic for up to 2700 days and overpredicts the early column density. These issues can be reconciled if one assumes a clumpy CSM shell. We note that asymmetry and clumping are important, so it is difficult to fit a convincing model for both the X-ray and radio emission.

Chugai & Chevalier (2006) in their original analysis had considered two models: one where the shock had overtaken the dense shell by the time X-ray observations commenced and another where the shock was still in the dense shell. Since the data at that time covered only the first 1000 days, they could not distinguish between the two models. Our fits to radio observations suggest evolution in Phase – 2 but do not show when Phase – 2 ended. The indications for this come from the X-ray observations. The X-ray light curves start to decline faster after the *XMM*-Newton epoch (i.e. 1735 days), suggesting that Phase-3 already started at this epoch (Fig. 11). The fast decline suggests a change in the ejecta-CSM interaction evolution. We suggest that the SN ejecta interacted with the dense shell until or before the *XMM*-Newton epoch and then the shock came out of the shell and started running through a faster declining CSM.

5.2. *Masses in the cool dense shell and the CSM H-shell*

We estimate the masses in various components of shocks and shells. The radio data are best fit by a combination of internal and external FFA, with a dominant contribution from internal FFA. Internal FFA is possible if a fraction of the cold gas is mixed in the radio emitting region. This is similar to what seen in SN 1986J where

the SN radio light curves were best fit with the internal absorption model mixed with external absorbers Weiler et al. (1990). The fact that the spectral index evolution is similar in both SNe (Fig. 8) suggests that similar mechanisms determine the light curves. Similar results have been found for other SNe IIn, e.g., SN 1988Z (van Dyk et al. 1993; Williams et al. 2002) and SN 2006jd (Chandra et al. 2012). In SN 2006jd, Chandra et al. (2012) calculated that a modest amount of cool gas mixed into the emitting region was sufficient to give rise to the needed absorption.

In the case of SN 2001em, we can do a rough estimate of the amount of mixing of the thermal absorber in the synchrotron emitting region if we assume the absorbing gas is in pressure equilibrium with the X-ray emitting gas and that it has a relatively low temperature ($10^4 - 10^5$ K). We calculate the mass loss when there is an optical depth of unity at 8.46 GHz, at an age of ~ 960 days. The mass-loss rate at this epoch is $\sim 2 \times 10^{-3}\, M_\odot\, \mathrm{yr}^{-1}$, corresponding to a circumstellar density of 9.3×10^5 cm^{-3}. The X-ray producing shock has an estimated temperature of ~ 20 keV, corresponding to a shock speed of $v_s \sim 4000$ km s^{-1}. Following the analogy of SN 2006jd (Chandra et al. 2012), a small amount of mixing of cool gas, i.e. $\leq 10^{-8}\, M_\odot$ can give rise to the needed absorption. The source of the cool gas is likely to be radiative cooling of dense gas in the shocked region, suggesting that the cool shell likely formed between the forward and the reverse shock.

We can also estimate the mass and energetics of the dense CSM shell. The observed shell interaction occurred roughly between days 764 and 1735. If we assume that the shock entered the dense shell not long ago before the first observations, then the duration of interaction is around 1000 days. For a velocity of the forward shock of 4000 km s^{-1}, the corresponding shell width is 3.5×10^{16} cm. Our estimate of the density 9.3×10^5 cm^{-3} implies the mass of the shocked CSM in the shell is $M_{\rm shell} \sim 2.5\, \mathrm{M}_\odot$. The total kinetic energy of the swept up material is $\sim E_{\rm shell} = 0.5 M_{\rm shell} v_{\rm FS}^2 \sim 4 \times 10^{50}$ erg.

5.3. *Late time spectrum of SN 2001em*

We have late time data at around day 5460, day 6670 and day 6872. We combine the last two epochs to create a wide band radio spectrum at an average epoch of day 6772.. The standard radio emission model for supernovae predicts optically thin spectra at these late stages. At day 5460, the spectra cover the frequency range 3–11 GHz and the spectrum is optically thin. On day 6772, the spectrum covers a frequency range of 0.4–32 GHz. Visually, the spectra are optically thin up to around 6 GHz, become optically thick, and then have a second transition to an optically thin phase at around 15 GHz. To estimate the robustness of these two transitions, we carry out Markov Chain Monte Carlo (MCMC) fitting using the Python package emcee (Foreman-Mackey et al. 2013). We choose 200 walkers, 1000 steps, and flat priors on all of the parameters. We obtain best-fit values (at 68% confidence interval, i.e., 1σ). We fit a smoothed broken powerlaw model with two break frequencies, as well

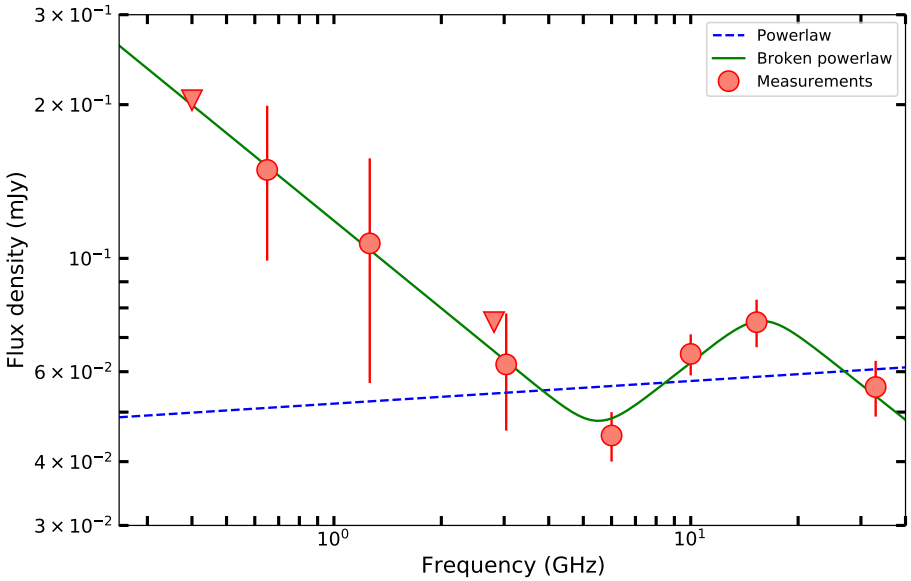


Figure 12. Day 6800 radio spectrum of SN 2001em. We carried out an MCMC analysis to fit a simple powerlaw and a double broken powerlaw model.

as a single powerlaw model (Fig. 12). A single powerlaw model results in an index of $0.04^{+0.08}_{-0.08}$ with a reduced $\chi^2 = 3.3$. The broken powerlaw results in indices between transition frequencies to be $-0.57^{+0.08}_{-0.08}$, $+0.56^{+0.03}_{-0.04}$ and $-0.55^{+0.07}_{-0.09}$, respectively with a reduced $\chi^2 = 0.89$. We show the fits in Fig. 12, indicating that the significance of the transitions seen in the spectrum is quite robust.

The late time spectrum in SN 2001em is quite similar to that of SN 1986J (Fig. 13). In SN 1986J, the spectrum at low frequencies had the form of a simple power law typically seen for SNe, with spectral index, $\alpha \approx -0.5$, but the radio emission was partly absorbed at high frequencies. Late VLBI observations showed a dominant central component (Bietenholz & Bartel 2017). In this scenario the best interpretation for SN 2001em is that the low frequency optically thin emission is from the fast shocks, whereas the rising spectrum at higher frequencies unveils the hidden central absorbed component as in SN 1986J.

5.4. *A common envelope scenario?*

In general, some supernova remnants have been shown to expand in W-R bubbles, before hitting the dense shell created by slow red-supergiant winds. However, in normal cases, the W-R bubble radius is around 10–12 pc, and the SN shock takes around 800–900 years to reach the shell (Dwarkadas 2005). In SN 2001em, and a few other known cases, the shock hits the shell in a few hundred days, i.e. the outer envelope was lost only a few thousand years before the explosion. How do these supernovae lose their envelope so close to explosion is not clearly understood. Our mass-loss rate estimate, $\sim (1-5)\times 10^{-3}\,\mathrm{M_\odot\,yr^{-1}}$, is high for such late time interaction. The supernova lost a $\sim 2.5\,\mathrm{M_\odot}$ H-envelope.

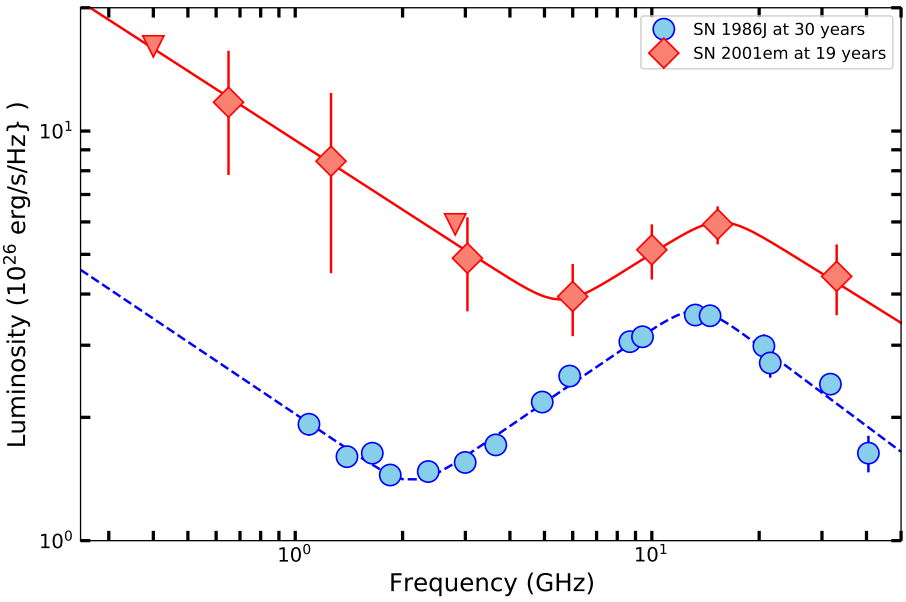


Figure 13. Comparison of the late time radio spectrum of SN 2001em at $\sim$ 19 yrs with that of SN 1986J at $\sim$ 30 yrs, which showed the presence of a central component at late times (Bietenholz & Bartel 2017).

This is a very large mass to be lost and the mechanism for the mass loss is not clear. Such large mass loss does occur during giant eruptions of Luminous Blue Variables (LBVs); η Carina is an example. Interestingly, a binary merger has been suggested for η Carina, in which there is a dense disk in the orbital plane and faster, lower density regions away from the plane (Smith et al. 2018) However, the LBV phase is generally not expected to be close in time to a supernova. A binary scenario involving a neutron star is a possible option, in which an in-spiraling neutron star causes mass loss followed by an explosion when it gets to the center of the star (Chevalier 2012). We suggest below that this could be a plausible scenario, support for which comes from the late time radio observations.

The explanation of the unusual spectrum in SN 1986J is that the radio was dominated by the standard optically thin expanding shell at low frequencies. The partially absorbed high frequency emission was dominated by the central component seen in VLBI observations, which eventually became optically thin at even higher frequencies. This behaviour might be explained by a common-envelope scenario in which a highly structured CSM is produced by a binary companion, as suggested by Chevalier (2012). In this scenario, the ejecta are initially optically thick, and the ejecta expanding above and below the equatorial disk initially absorb emission arising in these regions. After a time delay the central disk can be seen and the radio central component starts to reveal itself. In SN 1986J the central component was explained to be due to the SN shock interacting with the highly structured CSM produced by a binary companion, where the shock travelled much more slowly in the denser parts of the CSM near the binary orbital plane, thus producing a bright but compact

radio emission region (Bietenholz & Bartel 2017). A similar explanation may hold for SN 2001em. To investigate the relation between SN 1986J and SN 2001em, we overplot the spectrum of SN 1986J at 30 years with that of SN 2001em on day 5400 (Fig. 13). The similarity between the spectra in the overlapping frequency range is remarkable.

The common envelope scenario can also explain the loss of a $2.5\,M_{\odot}$ envelope, as the high mass loss is driven by common envelope evolution of a compact object in the envelope of a massive star and the SN explosion is triggered by the inspiral of the compact object to the central core of the companion star.

A prediction of a common envelope scenario is an asymmetric CSM. Our X-ray data provide evidence of asymmetry. Continuing radio observations over a wide band are needed to follow the spectrum of SN 2001em at late epochs to see whether there is evolution toward optically thin emission as is observed in SN 1986J.

5.5. *Comparison with normal SNe IIn*

In Fig. 14, we compare the SN 2001em 8 GHz spectral luminosity light curve with those of published SNe IIn light curves. SN 2001em is the second brightest radio supernova among the class of observed SNe IIn. Radio emission in SNe IIn is quite intriguing and most of the SNe IIn seem to become detectable at late epochs, after a few hundred days. This can partly be attributed to observational bias as some of the SNe IIn were either discovered late or observed late. For example, the prototypical SNe IIn SN 1986J, SN 1988Z and SN 1978K were discovered/observed years after their explosions. Many of the SNe IIn discovered sooner were not observed early enough in radio bands. However, SN 2010jl radio observations started by day 45, but the first radio detection was reported after 500 days, which Chandra et al. (2015) attributed to efficient absorption of radio emission at early epochs. SN 2009ip is the only exception. It was detected in radio bands early on but faded below detection within a few tens of days. However, SN 2009ip was a peculiar explosive event (Margutti et al. 2014).

Thus late radio turn on in SNe IIn, with the exception of SN 2009ip, is a common phenomenon. It remains to be seen in how many cases it can be attributed to high density absorption, and in how many cases due to late discovery/classification. For SN 2001em, the frequency dependence of the radio evolution indicates that absorption plays a role in the evolution.

The forward shock X-ray luminosity of a supernova, in an ideal case with no cooling and bremsstrahlung emission in a steady wind environment, is expected to decrease as t^{-1}. We observe a faster decline in the X-ray flux at the late stages of SN 2001em and interpret this as the shock moving into a medium with steeper density decline than $s = 2$. Dwarkadas & Gruszko (2012) found that the evolution expected for interaction with an $s = 2$ steady wind is rarely seen in supernovae, especially SNe IIn.

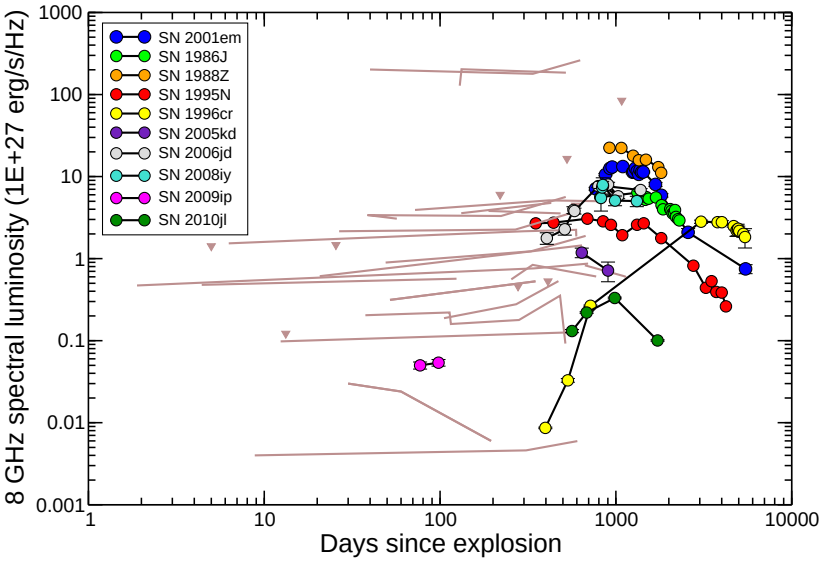


Figure 14. Comparison of the SN 2001em 8 GHz radio spectral luminosity to some of the well observed SNe IIn. Circles are detections; the lines indicate upper limits for observations at many epochs. Single triangles indicate upper limits at individual epochs (supernovae that were observed only once).

In Fig. 15, we plot 0.2–10 keV X-ray light curves of various SNe IIn. We also compared the behaviour of SN 2001em with older SNe IIn, which had most of the observations in the ROSAT soft X-ray bands. For this comparison, we obtained the SN 2001em flux in the 0.5–2.5 keV energy range. SN 2010jl, SN 2006jd and SN 2005kd also show fast declining evolution. SN 2010jl showed a flat evolution for the first 300 days followed by a more rapid decline. SN 1988Z and SN 1970G also show very steep X-ray evolution. The luminosity evolution of SN 1988Z shows a decline slope of -2.6 ± 0.6 (Schlegel & Petre 2006). In SN 1970G, the slope was -2.7 ± 0.9 (Immler & Kuntz 2005). SN 1986J was caught much later but it also revealed a steep luminosity decline (Houck 2005). Since the shock is expected to undergo adiabatic cooling and the temperature is expected to move to lower values, one does not expect a steepening at late times due to spectral constraints of the telescopes. The most plausible mechanism is that the shock is moving into a lower density medium with $s > 2$. In SN 2010jl, Chandra et al. (2015) also attributed the faster decline to a more rapidly decreasing circumstellar density profile. However, in some cases different parameters could give a situation in which the reverse shock wave has moved in to the flat part of the ejecta density distribution, which would also give a more rapid decline (Ofek et al. 2014).

5.6. *Comparison with supernovae undergoing metamorphosis*

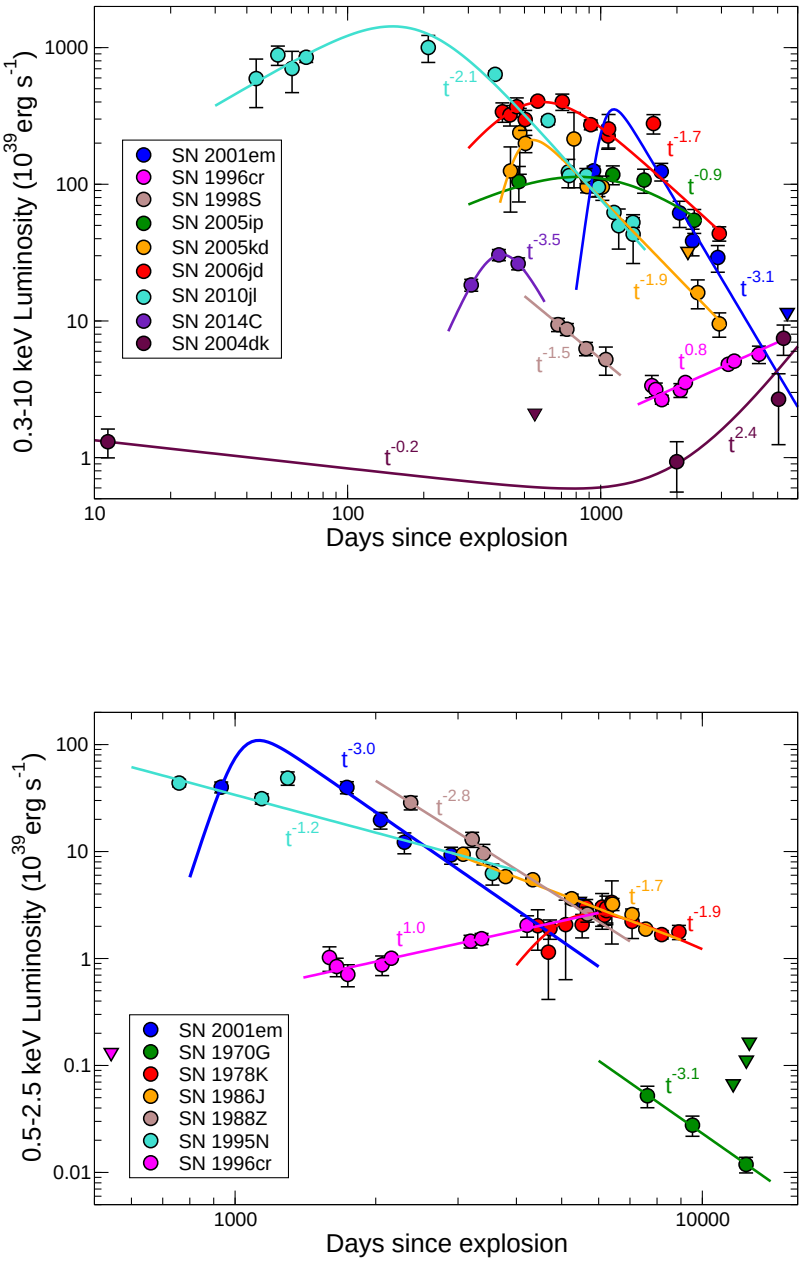


Figure 15. Comparison of the SN 2001em X-ray light curve with several other well observed light curves of interacting SNe IIn. The top panel shows the SNe IIn which have measured fluxes in the 0.2–10 keV energy range. The bottom panel shows SNe IIn in the soft energy band, which are mainly old SNe IIn observed with ROSAT. For comparison, we have estimated the SN 2001em flux in the soft energy band by using the fit parameters in Table 2. Many supernovae deviate from the standard $1/t$ dependence. The early evolution of SN 2001em is poorly constrained.

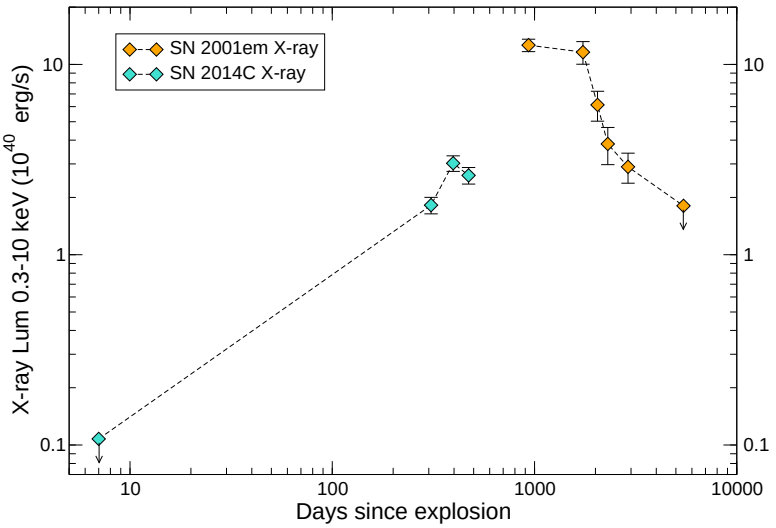


Figure 16. X-ray evolution of SN 2001em compared with that of SN 2014C (Margutti et al. 2017). With its early data, SN 2014C provides a complementary point of comparison to SN 2001em.

SN 2001em is an example of a class of core-collapse supernovae that fill a gap between events that interact strongly with nearby environments immediately after explosion (Type IIn and Ibn) and events that are not observed to interact. In SN 2001em, the interaction started after a few hundred days when the shock caught up to the ejected outer H layers of the pre-SN progenitor star. The details of shedding the outer layers in massive stars are not well known, though the common-envelope scenario is a possible mechanism in SN 2001em.

SN 2014C is a younger counterpart of SN 2001em that also had a stripped-envelope progenitor, and started showing similar signs of interaction by day 100 (Milisavljevic et al. 2015). Margutti et al. (2017) found that in the case of SN 2014C, the 1 $M_\odot$ H-shell was ejected only decades to centuries before the SN explosion. SN 2001em has revealed slower evolution, and the mass-loss episode leading to the shell happened $200-400$ years prior to the explosion. Possible reasons are that the shell was ejected much earlier in SN 2001em or that the progenitor winds were faster and accelerated the shell more rapidly. The early observations of SN 2014C complement SN 2001em and may give a qualitative picture of these SNe at early stages (Fig. 16).

SN 2004dk is another case of metamorphosis. SN 2004dk was a stripped envelope supernova with very detailed radio observations that revealed late time rebrightening (Wellons et al. 2012). Its X-ray luminosity around 13 days was 2×10^{39} erg s^{-1} (Wellons et al. 2012). Deep late-time optical spectroscopy at 4684 days showed Hα features, revealing that the shock caught up with the lost H (Mauerhan et al. 2018b). Pooley et al. (2019) presented observations spanning 15 years in X-rays. They esti-

mated that the shell of H-rich wind material was ejected $\sim$ 1400 years prior to the explosion, during carbon burning.

SN 2017ens was also a broad-line Type Ic supernova that changed into a Type IIn supernova with 2000 $\mathrm{km\,s^{-1}}$ Hα emission with a high luminosity $L_{\mathrm{H}\alpha} = 3 \times 10^{40}\,\mathrm{erg\,s^{-1}}$(Chen et al. 2018). Another example is SN 2005bf which was an unusual stripped envelope supernova (Folatelli et al. 2006): the explosion of a massive He star with a trace of a hydrogen envelope (Anupama et al. 2005). A Keck spectrum taken $\sim$ 233 days after explosion showed strong, broad Hα emission similar to SN 2001em. van Dyk (2010) suggested SN 2005bf and SN 2001em to be cases of a very massive star that experienced a powerful LBV eruption before evolving to the WR phase prior to explosion. Peculiar supernova SN 1996cr was initially identified as an ultraluminous X-ray source known as Circinus X-2, but later classified as a core collapse SN of Type IIn (Bauer et al. 2008). Dwarkadas et al. (2010) carried out detailed modeling and interpreted SN 1996cr as exploding in a low-density medium before interacting with a dense CSM shell, caused by the interaction of a blue supergiant or Wolf-Rayet (W-R) wind with a previously existing red supergiant (RSG) wind, 0.03 pc away from the progenitor star. The data also revealed that the shock wave has now exited the shell and is expanding into a medium that is consistent with the undisturbed continuation of the dense RSG wind. Another case is SN 2012ca. While initially it was thought to be a thermonuclear supernova, Public ESO Spectroscopy Survey of Transient Objects (PESSTO) nebular spectroscopy suggested it to be a stripped-envelope core collapse event, showing signs of interaction later on (Inserra et al. 2014). SN 2012ca was marginally detected in X-rays (Bochenek et al. 2018).

A radio survey of stripped envelope SNe at late time carried out by Bietenholz (2014) revealed that these SNe are few, yet the handful of examples pose questions for current theories of massive star evolution. Vinko et al. (2017) carried out a long-term survey of hydrogen-poor supernovae, with the aim of discovering late-time interaction and finding the hydrogen envelope expelled from the progenitor star several decades/centuries before the explosion. They detected continuum subtracted Hα emission in 9 SN Ibc, 1 SN IIb, and 3 SN Ia events. Similarly Margutti et al. (2017) found luminous radio rebrightening in SN 2003gk, SN 2007bg, and SN iPTF11qcj, attributing it to the ejecta-CSM collision. These examples indicate that there is probably a continuum between stripped envelope supernovae to hydrogen rich interacting supernovae.

5.7. *Similarities with SN 1986J*

SN 1986J deserves special attention due to it's similarities with SN 2001em. It was discovered a few years after the explosion (Rupen et al. 1987), so it is unclear whether it was a Type IIn supernova or a stripped-envelope supernova which underwent metamorphosis. Both supernovae are best fit with a $s = 2$ medium and the

internal absorption is dominant in both cases (Weiler et al. 1990). Fig. 8 shows the evolution of spectral indices in the two supernovae, which is strikingly similar.

In the other younger cousin, SN 2014C, the ejecta speed was much higher than that of SN 2001em; the expansion speeds were similar in SN 2001em and SN 1986J. The VLBI measurements for SN 2001em resulted in an expansion speed of < 6000 $\mathrm{km\,s^{-1}}$(Schinzel et al. 2008; Bietenholz & Bartel 2005), SN 1986J was found to have an expansion speed at around 1000 days to be $5700\,\mathrm{km\,s^{-1}}$(Bietenholz et al. 2004).

The most striking similarity is in the radio spectra at late epochs (Fig. 13). VLBI observations have ascertained that in SN 1986J, this optically thick spectrum is arising from a different interior component which is unveiled at a later time due to decreasing absorption (Bietenholz & Bartel 2017). A common-envelope scenario is a possible explanation for both supernovae (Chevalier 2012). Thus SN 2001em is most likely the younger cousin of SN 1986J.

6. CONCLUSIONS

SN 2001em is the oldest known SN to undergo metamorphosis from non-interacting to interacting supernova. Its long term study has provided us a unique opportunity to probe its pre-explosion history. Comprehensive analysis of radio and X-ray data indicate that the SN 2001em ejecta entered the shell before the first radio observations around 760 days, i.e. the end of Phase-1. The SN ejecta subsequently shocked the dense shell for around 1000 days. After around 1700 days the forward shock wave came out of the shell and started moving in the fast declining wind. Signatures of this behavior are seen in the X-ray observations. Our modelling suggests that radio and X-ray emission are primarily arising from the forward shock. Both radio and X-ray measurements reveal asymmetry and clumpiness in the ejecta and the CSM medium. One of the most interesting features is the optically thick radio spectrum after around 5000 days, which can be interpreted to be coming from a central component, similar to that seen in SN 1986J. Common envelope evolution may have played a role in producing the dense surroundings. The late time observations have given a new twist in the story of SN 2001em. We will be able to probe it further with future observations.

We thank referee for very useful comments which improved the manuscript significantly. PC acknowledges the support from the Department of Science and Technology via SwarnaJayanti Fellowship awards (DST/SJF/PSA-01/2014-15). RAC acknowledges support from NSF grant AST-1814910 and from NASA through Chandra award number AR8-19007X issued by the Chandra X-ray Center. The Chandra Center is operated by the Smithsonian Astrophysical Observatory for and on behalf of NASA under contract NAS8-03060. The National Radio Astronomy Observatory is a facility of the National Science Foundation operated under cooperative agreement by Associated Universities, Inc. This research has made use of data obtained through the High Energy Astrophysics Science Archive Research Center Online Service, provided by the NASA/Goddard Space Flight Center. We thank the staff of the GMRT that

made these observations possible. The GMRT is run by the National Centre for Radio Astrophysics of the Tata Institute of Fundamental Research. This work made use of data supplied by the UK Swift Science Data Centre at the University of Leicester.

Facilities: CXO, Swift(XRT), VLA, GMRT, XMM

REFERENCES

Anupama, G. C., Sahu, D. K., Deng, J., et al. 2005, ApJL, 631, L125

Arnaud, K. A. 1996, in Astronomical Society of the Pacific Conference Series, Vol. 101, Astronomical Data Analysis Software and Systems V, ed. G. H. Jacoby & J. Barnes, 17

Bauer, F. E., Dwarkadas, V. V., Brandt, W. N., et al. 2008, ApJ, 688, 1210

Bietenholz, M. F. 2014, PASA, 31, e002

Bietenholz, M. F., & Bartel, N. 2005, ApJL, 625, L99

—. 2007, ApJL, 665, L47

—. 2017, ApJ, 851, 7

Bietenholz, M. F., Bartel, N., & Rupen, M. P. 2004, Science, 304, 1947

Bochenek, C. D., Dwarkadas, V. V., Silverman, J. M., et al. 2018, MNRAS, 473, 336

Cash, W. 1979, ApJ, 228, 939

Chandra, P. 2018, SSRv, 214, 27

Chandra, P., Chevalier, R. A., Chugai, N., et al. 2012, ApJ, 755, 110

Chandra, P., Chevalier, R. A., Chugai, N., Fransson, C., & Soderberg, A. M. 2015, ApJ, 810, 32

Chandra, P., & Kanekar, N. 2017, ApJ, 846, 111

Chen, T. W., Inserra, C., Fraser, M., et al. 2018, ApJL, 867, L31

Chevalier, R. A. 1982, ApJ, 259, 302

Chevalier, R. A. 1996, in Astronomical Society of the Pacific Conference Series, Vol. 93, Radio Emission from the Stars and the Sun, ed. A. R. Taylor & J. M. Paredes, 125

—. 1998, ApJ, 499, 810

—. 2012, ApJL, 752, L2

Chevalier, R. A., & Fransson, C. 2017, Thermal and Non-thermal Emission from Circumstellar Interaction, ed. A. W. Alsabti & P. Murdin, 875

Chevalier, R. A., & Irwin, C. M. 2012, ApJL, 747, L17

Chevalier, R. A., & Liang, E. P. 1989, ApJ, 344, 332

Chugai, N. N., & Chevalier, R. A. 2006, ApJ, 641, 1051

Dwarkadas, V. V. 2005, ApJ, 630, 892

Dwarkadas, V. V., Dewey, D., & Bauer, F. 2010, MNRAS, 407, 812

Dwarkadas, V. V., & Gruszko, J. 2012, MNRAS, 419, 1515

Filippenko, A. V. 1997, ARA&A, 35, 309

Filippenko, A. V., & Chornock, R. 2001, IAUC, 7737, 3

Folatelli, G., Contreras, C., Phillips, M. M., et al. 2006, ApJ, 641, 1039

Foley, R. J., Smith, N., Ganeshalingam, M., et al. 2007, ApJL, 657, L105

Foreman-Mackey, D., Hogg, D. W., Lang, D., & Goodman, J. 2013, PASP, 125, 306

Fruscione, A., McDowell, J. C., Allen, G. E., et al. 2006, in Society of Photo-Optical Instrumentation Engineers (SPIE) Conference Series, Vol. 6270, 62701V

Granot, J., & Ramirez-Ruiz, E. 2004, ApJL, 609, L9

Grogin, N. A., & Geller, M. J. 2000, AJ, 119, 32

Harris, C. E., Nugent, P. E., & Kasen, D. N. 2016, ApJ, 823, 100

Hatchett, S., Buff, J., & McCray, R. 1976, ApJ, 206, 847

Houck, J. C. 2005, Astronomical Society of the Pacific Conference Series, Vol. 332, X-Ray Emission from SN 1986J, ed. R. Humphreys & K. Stanek, 429
Immler, S., & Kuntz, K. D. 2005, ApJL, 632, L99
Inserra, C., Smartt, S. J., Scalzo, R., et al. 2014, MNRAS, 437, L51
Kale, R., Parekh, V., & Dwarakanath, K. S. 2018, MNRAS, 480, 5352
Karamehmetoglu, E., Fransson, C., Sollerman, J., et al. 2019, arXiv e-prints, arXiv:1910.06016
Margutti, R., Milisavljevic, D., Soderberg, A. M., et al. 2014, ApJ, 780, 21
Margutti, R., Kamble, A., Milisavljevic, D., et al. 2017, ApJ, 835, 140
Mauerhan, J. C., Filippenko, A. V., Zheng, W., et al. 2018a, MNRAS, 478, 5050
—. 2018b, MNRAS, 478, 5050
McMullin, J. P., Waters, B., Schiebel, D., Young, W., & Golap, K. 2007, Astronomical Society of the Pacific Conference Series, Vol. 376, CASA Architecture and Applications, ed. R. A. Shaw, F. Hill, & D. J. Bell, 127
Milisavljevic, D., Margutti, R., Kamble, A., et al. 2015, ApJ, 815, 120
Modjaz, M., Liu, Y. Q., Bianco, F. B., & Graur, O. 2016, ApJ, 832, 108
Ofek, E. O., Zoglauer, A., Boggs, S. E., et al. 2014, ApJ, 781, 42
Papenkova, M., Li, W. D., Wray, J., Chleborad, C. W., & Schwartz, M. 2001, IAUC, 7722
Paragi, Z., Garrett, M. A., Paczyński, B., et al. 2005, Mem. Soc. Astron. Italiana, 76, 570
Pastorello, A., Smartt, S. J., Mattila, S., et al. 2007a, Nature, 447, 829
—. 2007b, Nature, 447, 829
Pooley, D., & Lewin, W. H. G. 2004, IAUC, 8323
Pooley, D., Wheeler, J. C., Vinkó, J., et al. 2019, ApJ, 883, 120
Prasad, J., & Chengalur, J. 2012, Experimental Astronomy, 33, 157
Puls, J., Vink, J. S., & Najarro, F. 2008, A&A Rv, 16, 209
Rupen, M. P., van Gorkom, J. H., Knapp, G. R., Gunn, J. E., & Schneider, D. P. 1987, AJ, 94, 61
Schinzel, F., Taylor, G. B., Stockdale, C. J., Granot, J., & Ramirez-Ruiz, E. 2008, in The role of VLBI in the Golden Age for Radio Astronomy, 94
Schlegel, D. J., Finkbeiner, D. P., & Davis, M. 1998, ApJ, 500, 525
Schlegel, E. M., & Petre, R. 2006, ApJ, 646, 378
Schrøder, S. L., MacLeod, M., Loeb, A., Vigna-Gómez, A., & Mandel, I. 2020, ApJ, 892, 13
Shiode, J. H., & Quataert, E. 2014, ApJ, 780, 96
Shivvers, I., Filippenko, A. V., Silverman, J. M., et al. 2019, MNRAS, 482, 1545
Smith, N. 2014, ARA&A, 52, 487
—. 2017, Interacting Supernovae: Types IIn and Ibn, ed. A. W. Alsabti & P. Murdin, 403
Smith, N., & Owocki, S. P. 2006, ApJL, 645, L45
Smith, N., Andrews, J. E., Rest, A., et al. 2018, MNRAS, 480, 1466
Soderberg, A. M., Gal-Yam, A., & Kulkarni, S. R. 2004, GRB Coordinates Network, 2586
Spitzer, L., & Arny, T. T. 1978, American Journal of Physics, 46, 1201
Stockdale, C. J., Van Dyk, S. D., Sramek, R. A., et al. 2004, IAUC, 8282
Stockdale, C. J., Kaster, B., Sjouwerman, L. O., et al. 2005, IAUC, 8472
van Dyk, S. D. 2010, in Astronomical Society of the Pacific Conference Series, Vol. 425, Hot and Cool: Bridging Gaps in Massive Star Evolution, ed. C. Leitherer, P. D. Bennett, P. W. Morris, & J. T. Van Loon, 73
van Dyk, S. D., Weiler, K. W., Sramek, R. A., & Panagia, N. 1993, ApJL, 419, L69
van Marle, A. J., Smith, N., Owocki, S. P., & van Veelen, B. 2010, MNRAS, 407, 2305
Vinko, J., Pooley, D., Silverman, J. M., et al. 2017, ApJ, 837, 62

Weiler, K. W., Panagia, N., Montes, M. J., & Sramek, R. A. 2002, ARA&A, 40, 387
Weiler, K. W., Panagia, N., & Sramek, R. A. 1990, ApJ, 364, 611
Wellons, S., Soderberg, A. M., & Chevalier, R. A. 2012, ApJ, 752, 17
Williams, C. L., Panagia, N., Van Dyk, S. D., et al. 2002, ApJ, 581, 396